CHEMISTRY
A EUROPEAN JOURNAL

DOI: 10.1002/chem.200401129

On the Influence of Charged Side Chains on the Folding–Unfolding Equilibrium of β-Peptides: A Molecular Dynamics Simulation Study

Alice Glättli,[a, d] Xavier Daura,[b] Pascal Bindschädler,[c, d] Bernhard Jaun,[c] Yogesh R. Mahajan,[c, d] Raveendra I. Mathad,[c, d] Magnus Rueping,[c, d] Dieter Seebach,[c] and Wilfred F. van Gunsteren*[a]

Abstract: The influence of charged side chains on the folding–unfolding equilibrium of β-peptides was investigated by means of molecular dynamics simulations. Four different peptides containing only negatively charged side chains, positively charged side chains, both types of charged side chains (with the ability to form stabilizing salt bridges) or no charged side chains were studied under various conditions (different simulation temperatures, starting structures and solvent environment). The NMR solution structure in methanol of one of the peptides (**A**) has already been published; the synthesis and NMR analysis of another peptide (**B**) is described here. The other peptides (**C** and **D**) studied herein have hitherto not been synthesized. All four peptides **A**–**D** are expected to adopt a left-handed 3_{14}-helix in solution as well as in the simulations. The resulting ensembles of structures were analyzed in terms of conformational space sampled by the peptides, folding behavior, structural properties such as hydrogen bonding, side chain–side chain and side chain–backbone interactions and in terms of the level of agreement with the NMR data available for two of the peptides. It was found that the presence of charged side chains significantly slows down the folding process in methanol solution due to the stabilization of intermediate conformers with side chain–backbone interactions. In water, where the solvent competes with the solute–solute polar interactions, the folding process to the 3_{14}-helix is faster in the simulations.

Keywords: molecular dynamics · molecular modeling · NMR spectroscopy · peptides · reversible folding

Introduction

The equilibrium of a polypeptide chain between its thermodynamically most stable conformation (the folded state) and all other thermodynamically accessible conformations (the unfolded state) depends on i) the thermodynamic conditions (temperature, pressure), ii) the environment (solvent, co-solvents, other solutes and pH), and iii) its amino-acid composition. To understand how the amino-acid sequence determines the three-dimensional structure of a peptide or protein, a shear number of studies has been undertaken to assess the secondary structure propensity of amino acids based on host–guest studies and database searches.[1–6] In the literature different explanations are proposed to rationalize the distinct preferences of amino acids for α-helical, β-strand and other conformational states. On the one hand, experimental[7–11] and theoretical[12] studies reveal that nonpolar side chains stabilize secondary structure elements and suggest that it is the hydrophobicity of amino acids which determines their conformational preferences. Similarly, electrostatic interactions between charged side chains, so-called salt bridges,[13–16] side chain–side chain hydrogen-bonding interactions, for example, between glutamine and aspara-

[a] Dr. A. Glättli, Prof. W. F. van Gunsteren
Laboratorium für Physikalische Chemie
Swiss Federal Institute of Technology
ETH Hönggerberg, HCI, 8093 Zürich (Switzerland)
Fax: (+41) 1-632-1039
E-mail: wfvgn@igc.phys.chem.ethz.ch

[b] Prof. X. Daura
Catalan Institution for Research and
Advanced Studies (ICREA) and Institute of Biotechnology and Biomedicine
Universitat Autònoma de Barcelona
08193 Bellaterra (Spain)

[c] P. Bindschädler, Prof. B. Jaun, Dr. Y. R. Mahajan, R. I. Mathad, Dr. M. Rueping, Prof. D. Seebach
Laboratorium für Organische Chemie
Swiss Federal Institute of Technology
ETH Hönggerberg, HCI, 8093 Zürich (Switzerland)

[d] Dr. A. Glättli, P. Bindschädler, Dr. Y. R. Mahajan, R. I. Mathad, Dr. M. Rueping
This work is part of the PhD thesis of A.G. (Diss. ETH No. 15609), Y.R.M. (Diss. ETH No. 15203, synthesis and characterisation of peptide B2), R.M. (NMR analysis of peptide B2) and of M.R. (Diss. ETH No. 14677, NMR analysis of peptide A) and of the master thesis of P.B. (synthesis and characterisation of peptide B2).

Supporting information for this article is available on the WWW under http://www.chemeurj.org/ or from the author.

gine[17,18] and side chain–backbone interactions at N- and C-termini (N- and C-capping)[19–21] have also been shown to stabilize helical conformations. On the other hand, Creamer and Rose[22–25] suggested that the loss in side-chain entropy upon folding in a defined secondary structure influences the α-helix propensities of amino acids most dominantly. In addition, unfavorable side chain–helix interactions (steric strain between side chains and the helix backbone) may also have an effect on helix propensities,[26–29] whereas β-sheet propensities seem to depend largely on the so-called side chain blocking effect, where large, bulky side chains interfere with hydrogen bonding between peptide and solvent and stabilize intramolecular hydrogen bonding.[30] Another approach to explain the secondary structure preferences of certain amino acid sequences is based on the backbone electrostatics: The stability of a conformational state is determined by local and nonlocal backbone electrostatic interactions, the strengths of which depend on the amino acid side chains and on the solvent.[31–33]

Based on this vast knowledge accumulated over the last two decades, protein design,[34] redesign[35] and the de novo design of isolated secondary structure elements by using natural[36] or nonnatural amino acids[37] has become a rapidly expanding area of protein science. Among the class of so-called foldamers, nonnatural compounds with a strong tendency to adopt specific three-dimensional conformations, β-peptides have attracted much attention in the past few years due to their remarkable stability towards common peptidases and their ability to form various stable secondary structure elements with as few as four β-amino acid residues.[38,39] Therefore, β-peptides are ideal model systems to study the process of folding and the secondary structure propensities of specific β-amino acid sequences.[38,40–42] The first β-peptides derived from homologues of natural α-amino acids carried aliphatic or benzylic side chains (Ala, Val, Leu, Phe) in the 2- and/or 3-position (substitution at the α- and/or β-carbon) and were shown by NMR and circular dichroism (CD) spectroscopy and by MD simulation to form 3_{14}-helices,[40,43–45] 10/12-helices[46,47] and hairpins[48,49] in methanol, analogous to the secondary structures of proteins. In order to understand the folding behavior of β-peptides in water, functionalized, charged side chains were incorporated in β-peptides to ensure high water solubility.[50–52]

Here, the folding–unfolding behavior of β-heptapeptides with functionalized side chains is studied by molecular dynamics (MD) simulation. In particular, the role of salt bridges in the stabilization of helices and the influence of charged side chains on the folding–unfolding equilibrium are investigated. To that end, we performed a series of simulations, summarized in Table 1, of four different peptides with different charged and aliphatic side chains, whose structural formulae are shown in Figure 1. Peptide **A** is soluble in

Table 1. Overview over the performed simulations, see also Figure 1.[a]

Peptide	Simulation name	Solvent	Number of solvent molecules	T [K]	Counterions present	Starting conformation	Simulation time [ns]
A	orn–glu$_{MeOH}$	MeOH	1728	298	–	extended	199
	orn–glu$_{H_2O}$	H_2O	3919	298	–	extended	99
B1	lys$_{298ext}$	MeOH	2144	298	–	extended	200
	lys$_{340ext}$	MeOH	2144	340	–	extended	200
	lys$^{*}_{298ext}$	MeOH	2141	298	3 Cl^-	extended	150
	lys$_{298hl}$	MeOH	1373	298	–	3_{14}-helix	100
	lys$^{*}_{298hl}$	MeOH	1370	298	3 Cl^-	3_{14}-helix	250
C	glu$_{298ext}$	MeOH	1920	298	–	extended	200
	glu$^{*}_{298ext}$	MeOH	1917	298	2 Na^+, 1 Cl^-	extended	100
D	val$_{298ext}$	MeOH	1862	298	–	extended	150
	val$_{340ext}$	MeOH	1862	340	–	extended	150

[a] Note that the simulation times indicated does not include the equilibration times of 1 ns. They refer to the time used for the analysis.

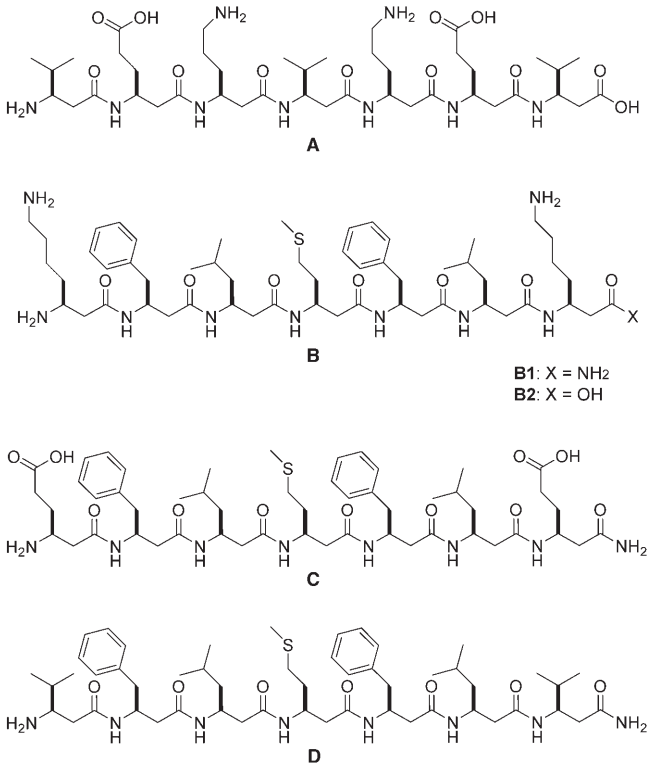

Figure 1. Chemical formulae of the β-heptapeptides **A**–**D** studied. Peptide **A**: H-β-HVal-β-HGlu-β-HOrn-β-HVal-β-HOrn-β-HGlu-β-HVal-OH; peptide **B**: H-β-HLys-β-HPhe-β-HLeu-β-HMet-β-HPhe-β-HLeu-β-HLys-X with X = -NH_2 for peptide **B1** and X = -OH for peptide **B2**; peptide **C**: H-β-HGlu-β-HPhe-β-HLeu-β-HMet-β-HPhe-β-HLeu-β-HGlu-NH_2; peptide **D**: H-β-HVal-β-HPhe-β-HLeu-β-HMet-β-HPhe-β-HLeu-β-HVal-NH_2. Peptide **B1**, with a C-terminal amide group, was investigated by MD simulation, while peptide **B2**, with a non-protected C-terminus, was studied experimentally. Note that in the simulations the N-termini, the ornithine (Orn) and lysine (Lys) residues are protonated, while the glutamic acid (Glu) residues and the carboxylic-acid C-terminus are deprotonated.[52,90]

water and methanol and has been shown by NMR and CD spectroscopy to adopt a 3_{14}-helix in both media. It contains two glutamic acid and two ornithine side chains, positioned in *i*,*i*+3 positions (where *i* indicates the residue number) allowing for the formation of two salt bridges in a 3_{14}-helical conformation.[52] Peptide **B** contains β^3-lysine residues located at the N- and C-terminus and was designed to test whether a β^3-heptapeptide without the α-branched side chains of Val or Ile[53,54] would adopt a 3_{14}-helical conformation in methanol. Preliminary CD spectroscopic experiments support the presence of 3_{14}-helical structures. In this simulation study peptide **B** was studied with a C-terminal amide group (henceforth denoted as peptide **B1**), while experimentally it was studied with a C-terminal carboxylic acid group (henceforth denoted as peptide **B2**). Although the different C-termini may influence the helical stability,[44,55] fundamental difference in the structural preference of the peptide with or without amide terminus is unlikely. Peptides **C** and **D** have not yet been synthesized, they are "derived" from peptide **B1** by replacement of the lysine by glutamic acid and by valine side chains, respectively. This would allow us to investigate the difference in behavior of β-peptides with positively and negatively charged side chains and to compare the influence of charged side chains on the folding–unfolding equilibrium to that of aliphatic side chains.

All four peptides were simulated in methanol solution at 298 K and 1 atm starting from a fully extended structure (Table 1) using the GROMOS package[56,57] and the GROMOS force field, version 45A3.[56,58] Peptide **A** was also simulated in aqueous solution (simulation orn–glu_{H_2O}), which offers the possibility to compare two different media. Additional simulations were performed, i) at elevated temperature (340 K) for peptides **B1** and **D** to access a larger part of conformational space and to sample more folding–unfolding events (simulations lys_{340ext} and val_{340ext}), ii) starting from a canonical 3_{14}-helix to further test the stability of the 3_{14}-helical conformation of peptide **B1** (simulations lys_{298hl} and lys^*_{298hl}), and iii) with additional neutralizing counterions to test the influence of counterions on the stability and folding behavior of peptides **B1** and **C** (simulations lys^*_{298ext}, lys^*_{298hl} and glu^*_{298ext}). The ensembles of structures from the trajectories were analyzed in terms of conformational space sampled by the peptide, folding behavior, structural properties such as hydrogen-bonding, side chain–side chain and side chain–backbone interactions and in terms of the level of agreement with the available NMR data. After presenting the simulation results of the four peptides individually in the Results section, the main observations made in all the 11 simulations are then compared and discussed in the Discussion section.

Results

Peptide A—Native fold is stabilized by salt bridges: Figure 2 shows the atom-positional root-mean-square deviation (rmsd) of the trajectory structures of the MD simulations of peptide **A** (sequence: H-β-HVal-β-HGlu-β-HOrn-β-HVal-β-HOrn-β-HGlu-β-HVal-OH) in methanol (a) and water (b) from the NMR model structure[52] as function of time along with the occurrence of the most dominant intramolecular hydrogen bonds. The hydrogen bonds observed in the simulations of peptide **A** correspond mostly to 14-membered rings characteristic for 3_{14}-helices. The hydrogen-bond populations of all peptides studied are summarized in Table 2. While in water peptide **A** folds to the experimentally determined 3_{14}-helix within the first 10 ns and subsequently unfolds and refolds to this conformation, the folding to a complete 3_{14}-helix in methanol takes more than 170 ns. Although the peripheral 3_{14}-helical hydrogen bonds, NH(1)−O(3), NH(4)−O(6) and NH(5)−O(7) are formed within the first 20 ns, the two central hydrogen bonds, NH(2)−O(4) and NH(3)−O(5), appear only after 170 ns. This corresponds to a relatively rapid formation of a partly folded 3_{14}-helix in methanol, which appears to be stable over more than 150 ns before it changes into a complete 3_{14}-helix.

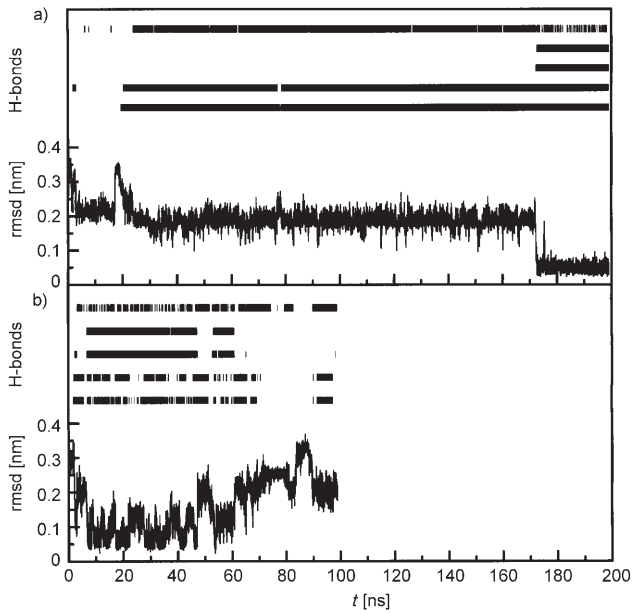

Figure 2. Atom-positional root-mean-square deviation (rmsd of backbone atoms of residues 2 to 6) of peptide **A** in a) methanol and b) water with respect to the 3_{14}-helical NMR model structure[52] along with the evolution of the hydrogen bonds characteristic of 3_{14}-helices. The hydrogen bonds displayed from top to bottom are NH(1)−O(3), NH(2)−O(4), NH(3)−O(5), NH(4)−O(6) and NH(5)−O(7). The definition of a hydrogen bond is given in the caption of Table 2. Due to low plotting resolution a hydrogen bond may be on average less present than implicated by the figure.

The populations (P) and the average lifetimes (τ) of the different conformations observed in the simulations were evaluated by a conformational clustering analysis described in the Methods section and are listed in Table 3, while the thermodynamic and kinetic folding properties of the 3_{14}-helix and of another helix, a 2.5_{12}-helix also observed in β-peptides, are summarized in Table 2. The structures of the three most populated conformers of peptide **A** in methanol

Table 2. Intramolecular hydrogen-bond populations [%].[a]

	Peptide **A**			Peptide **B1**				Peptide **C**		Peptide **D**	
Donor–acceptor	orn–glu$_{MeOH}$	orn–glu$_{H_2O}$	lys$_{298ext}$	lys$_{340ext}$	lys$^{*}_{298ext}$	lys$_{298hl}$	lys$^{*}_{298hl}$	glu$_{298ext}$	glu$^{*}_{298ext}$	val$_{298ext}$	val$_{340ext}$
NH(1)−O(3)	28	14	7	6	9	6	10	9	9	16	19
NH(2)−O(4)	12	40	2	7	3	4	36	27	24	46	51
NH(3)−O(5)	13	41	2	9	3	4	37	38	26	48	55
NH(4)−O(6)	78	37	10	9	17	7	38	41	28	56	64
NH(5)−O(7)	69	31	10	10	17	7	35	46	34	52	55
NH(1)−O(4)	11	11	8	3	8	7	2	7	9	6	8
NH(4)−O(7)	3	6	2	2	2	1	2	1	3	3	1
NH(1)−O(5)	3	4	3	2	3	2	0	9	6	4	2
NH(2)−O(6)	0	1	2	3	3	1	2	11	7	2	1
NH(3)−O(7)	0	1	3	3	2	6	2	2	0	1	2
NH(2)−O(7)	0	0	4	4	9	3	2	1	1	1	0
NH(5)−O(2)	0	0	7	2	0	1	5	0	7	2	1
NH(6)−O(3)	0	4	5	6	0	3	5	0	7	3	3
NH(7)−O(4)	0	0	4	5	1	3	4	1	4	3	2
NH$_C$(7)−O(5)	–	–	3	2	1	2	2	0	4	3	1
NH(2)−Glu(2)	13	1	–	–	–	–	–	–	–	–	–
NH(2)−Glu(6)	0	6	–	–	–	–	–	–	–	–	–
NH(3)−Glu(6)	0	6	–	–	–	–	–	–	–	–	–
NH(6)−Glu(6)	5	6	–	–	–	–	–	–	–	–	–
Orn(5)−Glu(2)	2	8	–	–	–	–	–	–	–	–	–
Lys(7)−O(4)	–	–	8	6	13	8	6	–	–	–	–
Lys(7)−O(5)	–	–	7	5	9	7	4	–	–	–	–
NH(1)−Glu(1)	–	–	–	–	–	–	–	15	14	–	–
NH(2)−Glu(7)	–	–	–	–	–	–	–	0	4	–	–
NH(3)−Glu(7)	–	–	–	–	–	–	–	7	6	–	–
NH(4)−Glu(7)	–	–	–	–	–	–	–	3	1	–	–
NH(7)–Glu(7)	–	–	–	–	–	–	–	9	8	–	–

[a] Only hydrogen bonds with a population larger than 3% in at least one of the simulations are reported. The hydrogen bonds are grouped according to the type of hydrogen bond (backbone-backbone or side chain-backbone hydrogen bonds) and the size of the resulting hydrogen-bonded ring (e.g. a hydrogen bond between NH of residue i and C=O of residue (i+2) results in a 14-membered hydrogen-bonded ring). The hydrogen-bond donor NH$_C$(7) corresponds to the C-terminal amide groups in the peptides **B1**–**D**. Side chain hydrogen bond donors or acceptors are indicated by the amino-acid residue names.

and water are displayed in Figure 3, together with the occurrence of their most dominant hydrogen bonds. The number of distinct conformers (N_{conf}) is quite low in both solvents (Table 3). The most populated conformer (75%) of peptide **A** in methanol corresponds to a partly unfolded 3_{14}-helix, while the complete 3_{14}-helix is only populated to the extent of 14%, representing the second most populated conformer in the simulation. In water the situation is reversed, with the 3_{14}-helix being populated for 49%, while only 20% of the sampled structures represent a partly unfolded 3_{14}-helix (Figure 3 and Table 3). This is in line with the results from the time evolution of the rmsd from the NMR model structure and the hydrogen-bond analysis presented above. Most lowly populated conformers correspond to randomly collapsed structures, as for instance the structure representing the third most populated conformer in methanol or water. The average lifetimes of the conformers in methanol are generally longer than in water, in particular the 3_{14}-helical conformation, which corresponds to cluster 2 in methanol and to cluster 1 in water, has a longer lifetime in methanol than in water (Tables 3 and 4). Even more pronounced is the difference in lifetimes of the partly unfolded 3_{14}-helix in the two solvent environments. In methanol, it is stable for an average of more than 10 ns, while the average lifetime in water is about 450 ps. In a similar way, the average folding time to the 3_{14}-helical conformation is much longer in methanol than in water (Table 4).

Figure 4 shows the distance between the ornithine and glutamic acid side chains as a function of time in methanol (a) and in water (b), together with the distance of the ornithine side chain of residue 5 and the C-terminus in both solvents (c). Only the distances between the charged side chains in an $i,i\pm3$ disposition are shown (Glu(2)−Orn(5) and Orn(3)−Glu(6)), since the interactions between these side chains are more sensitive to helix formation than the interactions between the side chains in $i,i\pm1$ positions. The distance between the latter pairs appears to be rather invariant with time. In methanol, the side chains of Orn(2) and Glu(5) approach each other within the first 5 ns of simulation but separate again before the second salt bridge between Orn(3) and Glu(6) is formed, which remains stable for the rest of the simulation. Only after more than 150 ns the salt bridge between Glu(2) and Orn(5) is reestablished along with the formation of the two central hydrogen bonds, NH(2)−O(4) and NH(3)−O(5), completing the folding into the experimentally observed 3_{14}-helix (compare Figure 4a with Figure 2a). A closer inspection of the transition from a partially unfolded to the fully folded 3_{14}-helix in methanol reveals that the formation of the central hydrogen bonds precedes the formation of the salt bridge between Glu(2)

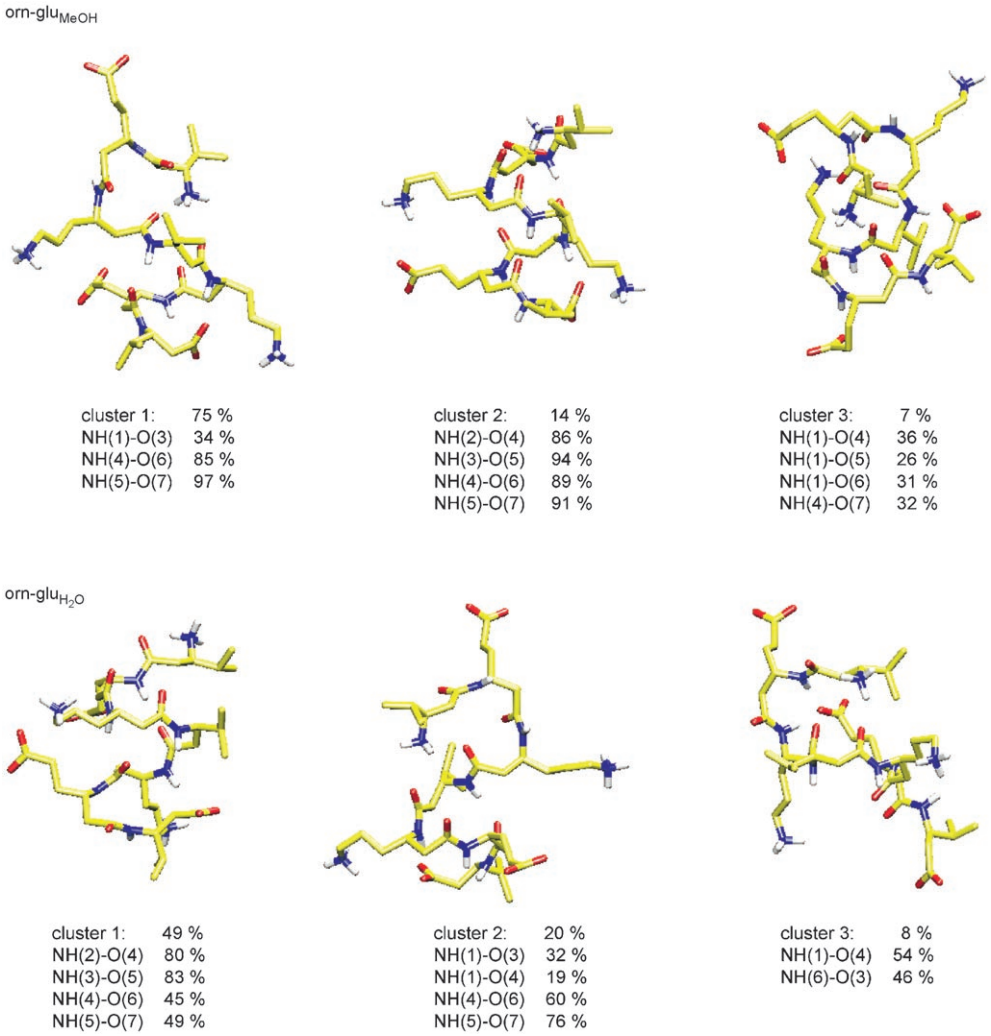

Figure 3. Three most populated conformers (central structures of the three most populated clusters using a backbone (residues 2–6) atom-positional root-meansquare difference (rmsd) similarity criterion of 0.1 nm) of peptide **A** observed in the simulations in methanol (orn–glu$_{MeOH}$) and in water (orn-glu$_{H_2O}$) at 298 K are shown (C = yellow, H = white, N = blue, O = red). For each conformer, its corresponding population and the occurrence of the most dominating hydrogen bonds are indicated. For nomenclature see caption of Table 2.

and Orn(5). This suggests that the salt bridges stabilize the overall structure of the peptide rather than being the driving force of folding to this structure. In water, both salt bridges are readily formed and disrupted upon (un)folding. Again the salt bridge between Orn(3) and Glu(6) is present more often than the one between Glu(2) and Orn(5), which is in agreement with the observation that the helix unfolds at the N-terminus in the second half of the simulation.

In addition to the formation of salt bridges between the charged side chains, backbone–side chain interactions are observed. In methanol the glutamic acid side chain of residue 2 (-COO^-) forms a hydrogen bond with the NH group of the same residue with a population of 13 % (Table 2) and the ornithine side chain of residue 5 (-NH_3^+) is observed to interact with the C-terminus of the peptide (-COO^-) for about 75 % of the simulation time (see Figure 4c) through a salt-bridge-like interaction. In water, the glutamic acid side chain of residue 6 is observed to form hydrogen bonds with the NH groups of residues 2, 3, and 6 all populated for 6 % (Table 2); the Orn(5) hydrogen binds to the side chain of Glu(2) for about 8 % of the simulation time. However, no persisting salt-bridge-like interaction between charged side chains and the peptide backbone is observed in water. It appears that these side chain-backbone interactions stabilize conformations other than the 3_{14}-helix. The effect is more pronounced in methanol (Figure 4c), a solvent with a much lower dielectric permittivity than water, where there is less competition between solute–solvent and solute–solute hydrogen bonding. This results in quite stable intermediate structures such as the partly unfolded 3_{14}-helix and might be the reason why the average lifetimes of the conformers are longer in methanol than in water.

We also compare the experimentally measured NOE intensities for peptide **A**, which were converted to NOE distances, and J values[52] with the values calculated from the structures in the simulations in methanol and water. From the total of 80 NOE distances in methanol and 64 in water, only the interresidue distances (29 and 21, respectively)

Table 3. Conformational clustering analysis for all simulations using an atom-positional root-mean-square difference of the backbone atoms (N, C_β, C_α, C) of residues 2–6 of 0.1 nm.[a]

	Conformational analysis: conformer populations and average lifetimes																					
	Peptide **A**					Peptide **B1**								Peptide **C**				Peptide **D**				
	orn–glu_{MeOH}		orn–glu_{H_2O}		lys_{298ext}		lys_{340ext}		lys^*_{298ext}		lys_{298hl}		lys^*_{298hl}		glu_{298ext}		glu^*_{298ext}		val_{298ext}		val_{340ext}	
	[%]	[ps]	[%]	[ps]	[%]	[ps]	[%]	[ps]	[%]	[ps]	[%]	[ps]	[%]	[ps]	[%]	[ps]	[%]	[ps]	[%]	[ps]	[%]	[ps]
$N^{conf}_{100\%}$	36		59		400		668		213		195		323		226		160		163		207	
$N^{conf}_{99\%}$	11		26		267		482		127		129		192		132		94		86		109	
$N^{conf}_{75\%}$	1		3		46		90		18		26		17		8		15		6		2	
$N^{conf}_{50\%}$	1		2		14		26		6		10		2		2		4		1		1	
Conformer	*P* [%]	τ [ps]	*P* [%]	τ [ps]	*P* [%]	τ [ps]	*P* [%]	τ [ps]	*P* [%]	τ [ps]	*P* [%]	τ [ps]	*P* [%]	τ [ps]	*P* [%]	τ [ps]	*P* [%]	τ [ps]	*P* [%]	τ [ps]	*P* [%]	τ [ps]
1	75	10654	49	3058	9	705	11	599	17	2065	11	162	46	4596	42	7013	28	4116	54	3679	64	2430
2	14	4468	20	446	7	330	3	122	13	367	8	1171	5	1656	15	2390	12	603	12	826	16	802
3	7	4633	8	221	6	132	3	285	9	813	8	7650	3	467	8	2642	6	315	3	414	3	189
4	1	1310	5	928	5	543	3	63	5	304	4	186	3	447	3	450	6	415	3	456	1	113
5	1	1430	3	73	4	158	3	173	4	1170	4	166	2	298	3	415	4	231	3	493	1	68
6	1	407	2	211	3	407	3	157	4	292	4	216	2	271	2	116	3	147	2	159	1	62
7	1	138	1	62	3	98	2	119	4	170	4	214	2	294	2	518	3	540	2	228	1	84
8	<1	280	1	72	2	1557	2	186	3	132	3	118	2	777	1	198	2	2460	1	272	1	310
9	<1	190	1	605	2	481	2	256	3	591	3	215	2	137	1	114	2	106	1	657	1	69
10	<1	240	1	133	2	2375	2	54	3	176	3	105	2	328	1	168	2	717	1	453	1	117

[a] The total number of conformers ($N^{conf}_{100\%}$) and the number of most populated conformers with a combined population of 99% ($N^{conf}_{99\%}$), 75% ($N^{conf}_{75\%}$), and 50% ($N^{conf}_{50\%}$) of the sampled conformational space is indicated for each simulation. For the 10 most populated conformers the populations *P* (in %) and average lifetimes τ [ps] are listed. The average lifetime of a conformer was calculated by recording the times at which the conformer was left and accessed again. If a conformer was left and accessed within 20 ps the sampling of the conformer was considered to be continuous. For further details see methods section and ref. [85].

were considered. The results are presented in the Supporting Information to this article. The simulation in methanol violates 14 out of the 29 interresidue NOE distances, which is certainly due to the fact that in methanol the peptide adopts for 75% of the simulation time a partly folded 3_{14}-helical conformation lacking the central hydrogen bonds, NH(2)−O(4) and NH(3)−O(5), that is, there is insufficient sampling. The positive violations are on average smaller when one considers only structures belonging to the second most populated cluster, which represents the 3_{14}-helical conformation. In order to better fulfil the NOE upper-bound distances in methanol the 3_{14}-helical conformation should be weighted more, as it is the case in the simulation in water, where the 3_{14}-helix is populated to the extent of 49% and only five inter-residue NOE distances are weakly violated. The calculated ^3J-coupling constants show an absolute average deviation of 0.4 Hz, both in methanol and in water. Using a conservative estimate of 0.7 Hz for the uncertainty when the ^3J coupling constants are calculated by using the Karplus equation [Eq. (1)] (see Methods Section),[59,60] the measured ^3J-coupling constants are reproduced in both simulations.

Peptides B—Lysine side chains compete with backbone–backbone hydrogen bonding: Peptide **B1** (sequence: H-β-HLys-β-HPhe-β-HLeu-β-HMet-β-HPhe-β-HLeu-β-HLys-NH_2) has been simulated starting from a fully extended conformation at room temperature (298 K) without and with the addition of neutralizing counterions (simulations lys_{298ext} and lys^*_{298ext}) and at elevated temperature (340 K) (simulation lys_{340ext}). In addition, two simulations at room temperature starting from a canonical 3_{14}-helix without and with the addition of counterions (simulations lys_{298hl} and lys^*_{298hl}) were performed in order to test the stability of the 3_{14}-helix. The hydrogen-bond analysis indicates, first of all, that none of the simulations of peptide **B1** shows sizeable intramolecular hydrogen bonding except for simulation lys^*_{298hl} (Table 2). Second, in most simulations of peptide **B1** not only hydrogen bonds characteristic of a left-handed 3_{14}-helix (NH(*i*)–O(*i*+2)), but also 12-membered hydrogen bonded rings (NH(*i*)–O(*i*−3)) characteristic of a right-handed 2.5_{12}-helix are observed. The rmsd from a 3_{14}-helix and from a 2.5_{12}-helix are shown in Figure 5, together with the most dominant backbone–backbone and side chain–backbone hydrogen bonds as a function of simulation time. The results of the conformational clustering analysis are listed in Table 3 and the structures of the three most dominant conformers of each simulation are displayed in Figures 6 and 7. The thermodynamic and kinetic folding properties of the helical conformations observed in the simulations (3_{14} and 2.5_{12}-helix) are presented in Table 4.

At 298 K (Figure 5a) peptide **B1** adopts, within the first 25 ns, a 2.5_{12}-helix and folds only after 110 ns into a 3_{14}-helical conformation, which unfolds again after less than 5 ns. The 2.5_{12}-helix reappears towards the end of the simulation. Consequently, the average folding time to the 3_{14}-helix is longer than the (re)folding time to the 2.5_{12}-helical confor-

Table 4. Thermodynamic and kinetic properties of the two helical conformations, the left-handed 3_{14}-helix and the right-handed 2.5_{12}-helix, observed in the simulations.[a]

Peptide	Simulation	Conformer ranking	Population [%]	τ [ps]	Number of folding events to 3_{14}-helix	⟨Time⟩ of folding to 3_{14}-helix	⟨Number of conformers⟩ visited during (re)folding
		Conformational analysis: left-handed 3_{14}-helix					
A	orn–glu_{MeOH}	2	14	4468	6	14385	5
	orn–glu_{H_2O}	1	49	3058	16	1158	5
B1	lys_{298ext}	8	2	1557	3	25329	95
	lys_{340ext}	1	11	599	39	5692	70
	lys^{*}_{298ext}	5	4	1170	5	7312	13
	lys_{298hl}	3	8	7650	–	–	–
	lys^{*}_{298hl}	1	46	4596	23	6631	22
C	glu_{298ext}	1	42	7013	12	10503	24
	glu^{*}_{298ext}	1	28	4116	7	10144	33
D	val_{298ext}	1	54	3679	22	2659	12
	val_{340ext}	1	64	2430	40	1110	10
		Conformational analysis: right-handed 2.5_{12}-helix					
Peptide	Simulation	Conformer ranking	Population [%]	τ [ps]	Number of folding events to 2.5_{12}-helix	⟨Time⟩ of folding to 2.5_{12}-helix	⟨Number of conformers⟩ visited during (re)folding
B1	lys_{298ext}	4	5	453	17	11568	34
	lys_{340ext}	8	2	186	28	5481	67
	lys^{*}_{298hl}	4	3	447	18	9968	29
C	glu^{*}_{298ext}	4	6	415	14	5002	16
D	val_{298ext}	5	3	493	8	25598	26
	val_{340ext}	8	1	310	3	2387	46

[a] The 2.5_{12}-helix was not observed in the simulations orn–glu_{MeOH}, orn–glu_{H_2O}, lys_{298ext}, lys_{298hl} and glu_{298ext}. For every simulation, the ranking with regard to population of the helical conformation, its population, average lifetime τ and number of (re)folding events is indicated together with the average time of (re)folding to the helix and the average number of conformations visited during a (re)folding process. The average lifetime and the number of (re)folding processes were calculated by recording the times at which the conformer was left and accessed again. If a conformer was left and accessed within 20 ps the sampling of the conformer was considered to be continuous. Only a subset of folding events involving more than one intermediate conformer was considered when calculating the average time of (re)folding and the average number of conformers visited during the (re)folding process. Averaging is denoted by ⟨…⟩.

mation (Table 4). Again, the central hydrogen-bonds characteristic of the 3_{14}-helix, NH(2)···O(4) and NH(3)···O(5), are much less populated than the terminal ones, similar to the situation of peptide **A** in methanol. It appears that the lysine side chains compete with the backbone NH groups as hydrogen-bond donors, forming hydrogen bonds with the carbonyl oxygen atoms of residue 4 and 5, populated at 8 and 7% (Table 2). Consequently, the most populated conformer (9% of total population) corresponds to a partially folded 3_{14}-helix (Figure 6), while the second and third most populated conformers (7 and 6% populated, respectively) show no regular structure. The 2.5_{12}-helix appears to be the fourth most populated conformer (5% populated, Table 2) and the complete 3_{14}-helix represents the eighth most populated conformer with a population of 2%.

The simulation lys_{340ext} at elevated temperature shows a similar picture, but the interconversion between 3_{14}- and 2.5_{12}-helical conformations occurs much faster (Figure 5b and Table 2). The 3_{14}-helix, which corresponds to the most populated conformer (11%) in the simulation lys_{340ext}, is sampled more often than at room temperature and is on average more stable than the 2.5_{12}-helix, which represents the eighth most populated conformer in the simulation (2% populated). The average folding times to the 3_{14}-helix and to the 2.5_{12}-helix at 340 K are both in the order of 5.5 ns.

The presence of neutralizing counterions in simulation lys^{*}_{298ext} seems to have no significant effect on the folding behavior of peptide **B1** (Figure 5c) except that no 2.5_{12}-helical conformations are sampled. Whether this is due to the counterions or simply an issue of undersampling is questionable, especially when considering the fact that in the simulation starting from a 3_{14}-helix with counterions the peptide refolds several times to a 2.5_{12}-helix (Figure 5e). In the simulations starting from a canonical 3_{14}-helix the replacement of methanol molecules with the largest Coulomb potential by counterions has a significant stabilizing effect. While in the simulation lys_{298hl}, where no counterions are present, the helix unfolds within the first 5 ns (Figure 5d), in simulation lys^{*}_{298hl}, where neutralizing counterions were added, the helix is stable for more than 70 ns. Once completely unfolded (i.e., to a structure with no 14-membered hydrogen-bonded rings), the refolding process to the 3_{14}-helix takes as long as in the simulations starting from an extended structure (more than 120 ns). Again, side chain–backbone interaction between the lysine side chains, Lys(7) in particular, and the carbonyl oxygen atoms of residue 4 and 5 as well as the formation of 12-membered hydrogen-bonded rings can be observed (Table 2 and Figure 8). However, in contrast to all other simulations of peptide **B1**, the 3_{14}-helix is stable and shows an average lifetime of 4.6 ns, comparable to the lifetime of 4.5 ns of the 3_{14}-helical conformation of peptide **A** in methanol (Table 3).

The conformational preference of peptide **B2** (C-terminal carboxylic acid group) in methanol has been studied by

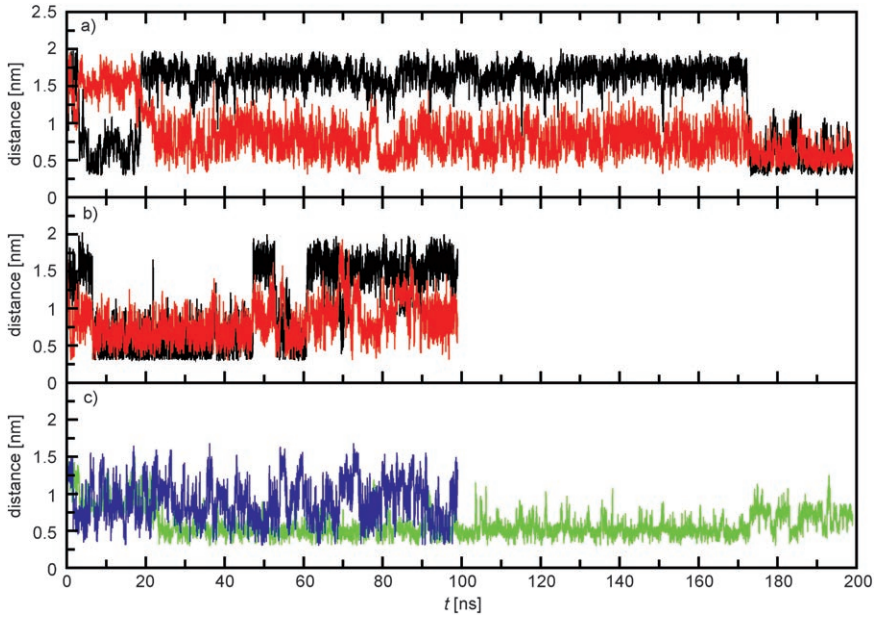

Figure 4. Salt-bridge formation and side chain-backbone interactions: The distances between the centers of geometry of side chain charge groups of Glu(2) and Orn(5) (black) and Orn(3) and Glu(6) (red) of peptide **A** are displayed as a function of time for the simulation in a) methanol and b) water. The formation of salt bridges between these side chains is considered to favor the 3_{14}-helical conformation. c) The distance between the ammonium group of the ornithine side chain of residue 5 and the C-terminus (-COO^-) is displayed for the simulation in methanol (green) and in water (blue).

NMR experiments (see Supporting Information) and the resulting NOE distances and measured ^3J values were used to compare with the values calculated from the simulations of peptide **B1** (C-terminal amide group). From the total number of 84 NOE distances inferred from experiment only 18 NOE distances correspond to interresidue distances. Only a few long-range (in sequence number) NOE distances are observed. In particular, neither long-range NOE signals between backbone amine groups (NH) nor NOE signals characteristic of a stable 3_{14}-helical conformation could be detected. This makes it impossible to derive a dominant structure for peptide **B2** from these data. On the other hand, the experimentally measured ^3J coupling constants indicate that the torsional dihedral angle C(O)-N-C_β-C_α preferentially adopts a anticlinal ((−)-ac) conformation (−120°), while the torsional dihedral angle N-C_β-C_α-C(O) appears to adopt a *gauche*(+) conformation (60°, (+)-sc), which correspond to the dihedral angle conformation in 3_{14}-helices. The comparison of the experimental NOE distances inferred from experiment and the measured ^3J values of peptide **B2** with the values calculated from each of the five simulation trajectories of peptide **B1** shows an overall satisfactory agreement (see Supporting Information for detailed results): Almost all sequential NOE distances are fulfilled in all five simulations, while all six long-range NOE bounds are violated in the simulations where the 3_{14}-helix is only weakly populated (simulations lys_{298ext}, lys_{340ext}, lys^*_{298ext} and lys_{298hl}). In the simulation lys^*_{298hl}, where the 3_{14}-helix is populated for 46% (Table 2), all long-range NOE bounds are fulfilled. The experimentally measured ^3J coupling constants are well reproduced by all five simulations. The calculated values show an average absolute deviation between 0.6 and 1.0 Hz (see Supporting Information), where the simulations lys_{298ext} and lys^*_{298hl} satisfy the experimental ^3J coupling constants overall better than the other three simulations (lys_{340ext}, lys^*_{298ext} and lys_{298hl}). It appears that in all five simulations the ^3J(NH,C_βH) coupling constants are better fulfilled than the ^3J(C_βH,C_αH) coupling values.

In summary, we found that a very large number of different conformers of generally rather low populations is observed. Consequently no conformer appears to be dominant in all but the simulation lys^*_{298hl} of peptide **B1**. Although two well-defined helical conformations, a left-handed 3_{14}-helix and a 2.5_{12}-helix, are observed, they both show relatively short lifetimes and low populations and thus are not very stable, unless stabilized by counterions as the 3_{14}-helix in simulation lys^*_{298hl}. Second, the time required to fold from a fully extended conformation to the 3_{14}-helix is in the order of 100 to 150 ns, comparable to the folding time observed for peptide **A** in methanol. The average folding times are relatively long and less folding–unfolding events are observed compared with peptides containing only aliphatic side chains (Table 2).[42] This slow folding behavior is probably due to the lysine side chain–backbone interactions (Figure 8), which are in direct competition with the central backbone–backbone hydrogen bonds NH(2)···O(4) and NH(3)···O(5), which are crucial in the stabilization of the 3_{14}-helix. Due to the relatively low dielectric permittivity of the methanol model used ($[\varepsilon]_{MeOH}$ = 17.7),[61] the positively charged lysine side chains might not be optimally solvated and may tend to repel each other whenever they come close, which probably destabilizes the helix if no counterions are in the vicinity of the lysine side chains to interact with.

Peptide C—The effect of negatively charged side chains: Replacing the lysine side chains in peptide **B1** by glutamic acid side chains offers the possibility to investigate the effect of negatively charged side chains. As all β^3-peptides (all side chains in the β-position of the amino acids) generally form 3_{14}-helices,[39,52,62,63] the resulting peptide **C** (sequence: H-β-HGlu-β-HPhe-β-HLeu-β-HMet-β-HPhe-β-HLeu-β-HGlu-NH_2, Figure 1), is expected to form a 3_{14}-helix. The hitherto not synthesized peptide **C** was simulated at 298 K, starting from a fully extended conformation with-

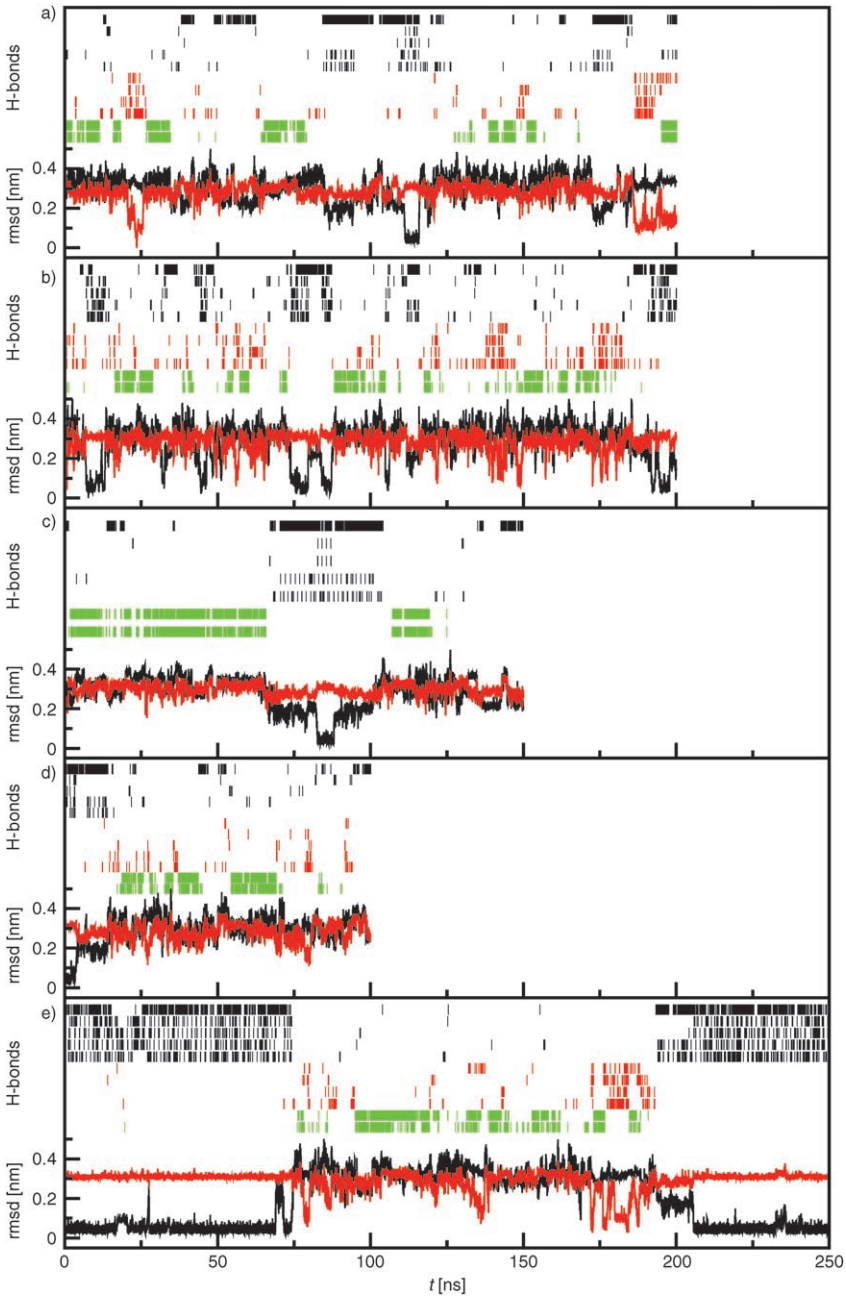

Figure 5. Backbone atom-positional rmsd with respect to a 3_{14}-helical conformation (black) and a 2.5_{12}-helix (red), the two main helical conformations observed in the simulations of peptide **B1**, along with the evolution of the most populated backbone-backbone and side chain-backbone hydrogen bonds. Black: NH(i)–O(i+2) hydrogen bonds characteristic of 3_{14}-helices displayed from top to bottom: NH(1)–O(3), NH(2)–O(4), NH(3)–O(5), NH(4)–O(6) and NH(5)–O(7). Red: NH(i)–O(i–3) hydrogen bonds characteristic of 2.5_{12}-helices displayed from top to bottom: NH(5)–O(2), NH(6)–O(3), NH(7)–O(4) and NHC(7)–O(5). NH_C corresponds to the C-terminal amide group. Green: Side chain–backbone hydrogen bonds between the lysine side chain in position 7 and the carbonyl oxygen atoms of residues 4 and 5 are displayed from top to bottom. a) simulation lys_{298ext}; b) simulation lys_{340ext}; c) simulation lys^{*}_{298ext}; d) simulation lys_{298hl}; e) simulation lys^{*}_{298hl}.

out and with the addition of neutralizing counterions (simulations glu_{298ext} and glu^{*}_{298ext}). The hydrogen-bond analysis over the two trajectories presented in Table 2 shows that mostly 14-membered hydrogen-bonded rings are formed. Hydrogen bonds characteristic of the 2.5_{12}-helix are only noticeably populated in the simulation with counterions (glu^{*}_{298ext}). Note that this is the reverse of the situation observed for peptide **B1**. There, the simulation without counterions (lys_{298ext}) showed a higher 2.5_{12}-helical propensity than the simulation with ions (lys^{*}_{298ext}). Comparing the rmsd from a 3_{14}-helix and a 2.5_{12}-helix of the two trajectories with the time evolution of the most dominant hydrogen bonds shows that in simulation glu_{298ext} (Figure 9a) the peptide forms a 3_{14}-helix at around 70 ns, quickly unfolds after 5 ns of simulation and refolds again to a stable 3_{14}-helix shortly after 100 ns. No formation of 2.5_{12}-helices is observed. In simulation glu^{*}_{298ext} (Figure 9b), however, the peptide is observed to first fold and refold to a 2.5_{12}-helix and then after 70 ns to adopt a 3_{14}-helix, which remains stable for the rest of the simulation. Consequently, the 3_{14}-helical conformation represents in both cases the most dominant conformer, while the second and third most populated conformers correspond to randomly collapsed structures with one 14-membered hydrogen bonded ring or partially folded 3_{14}-helices (Figure 10). In contrast to the simulations of peptide **B1** that did not start from a 3_{14}-helical structure, the 3_{14}-helical conformation is much more populated and shows on average a longer lifetime (Table 4). Side chain–backbone interactions such as hydrogen bonds are observed to some extent between the glutamic-acid side chains and the NH groups of the peptide backbone (Table 2). The folding behavior and the structural preference of peptide **C** appears to be rather independent of the presence of neutralizing counterions.

Peptide D—Peptide folding is a faster process without charged side chains: If the presence of charged side chains would slow down the folding kinetics of a β-peptide, the replacement of charged side chains by aliphatic ones should

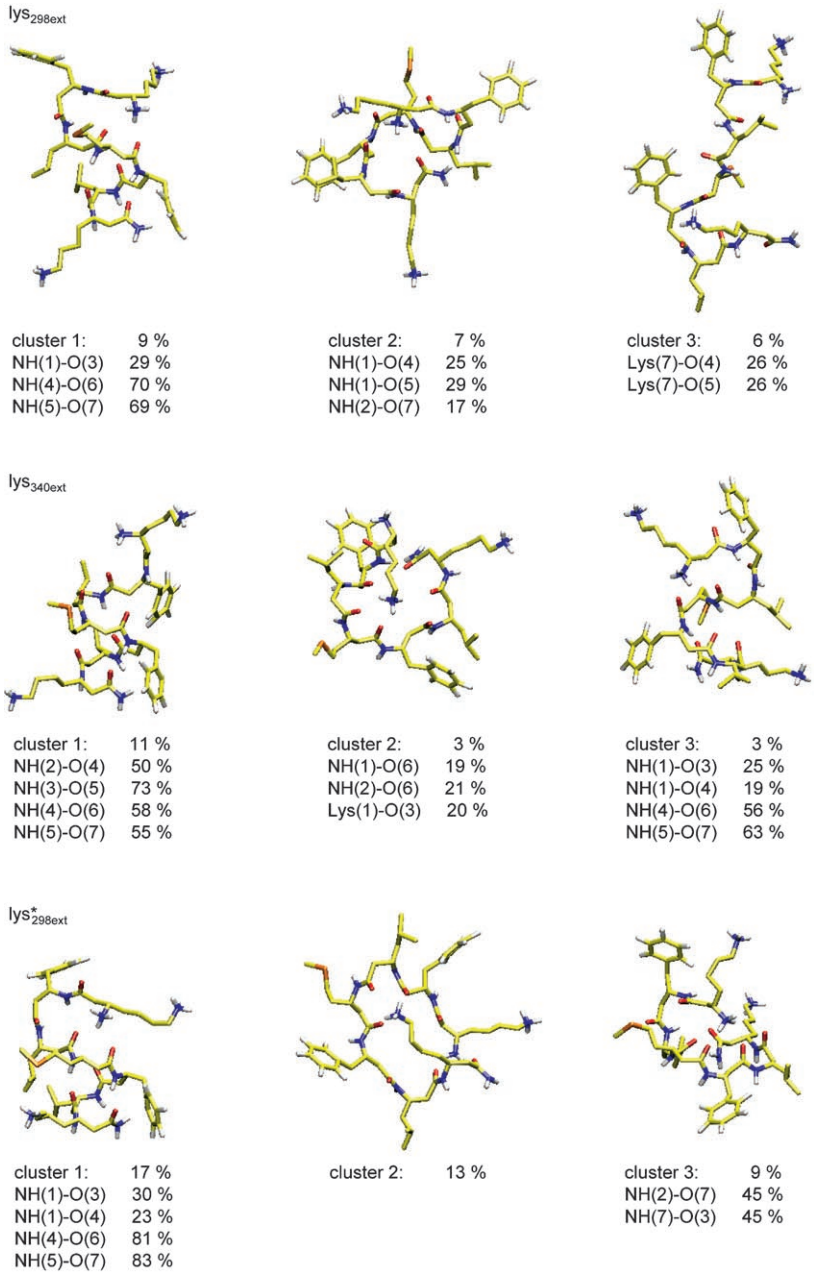

Figure 6. Three most populated conformers (central structures of the three most populated clusters using a backbone (residues 2–6) atom-positional rmsd similarity criterion of 0.1 nm) of peptide **B1** observed in the simulations lys_{298ext}, lys_{340ext}, lys^{*}_{298ext}, where the initial conformation was fully extended, are shown (C = yellow, H = white, N = blue, O = red, S = orange). For each conformer, its corresponding population and the occurrence of the most dominating hydrogen bonds are indicated. For nomenclature see caption of Table 2.

result in faster folding kinetics of the peptide. To test this assumption the charged side chains in peptides **B1** and **C** were substituted by valine side chains leading to peptide **D** (sequence: H-β-HVal-β-HPhe-β-HLeu-β-HMet-β-HPhe-β-HLeu-β-HVal-NH_2), which has not been synthesized, as yet, and which was simulated starting from a fully extended conformation both at 298 and 340 K (simulations val_{298ext} and val_{340ext}). The hydrogen-bond populations (Table 2), the conformational clustering analysis (Tables 3 and 4, Figure 12) and the rmsd values from a canonical 3_{14}-helix (Figure 11) show that the peptide's preferred conformation is a 3_{14}-helix, which forms within the first 20 ns in both simulations. Compared to the simulations with charged side chains, the population of the 3_{14}-helix is much larger and the average folding times taken to reach the 3_{14}-helix are shorter (Table 4). At both temperatures, 2.5_{12}-helices are sampled as well, but at much lower population representing cluster 5 at 298 K and cluster 8 at 340 K. The fact that at 340 K the 3_{14}-helix is 10% more populated than at room temperature does not necessarily mean that the helix is more stable at 340 than at 298 K. It is probably due to the fact that at lower temperature the interconversion between different conformers is slower. This makes convergence of the folding–unfolding equilibrium distribution slower: at 298 K only 22 folding events are observed, whereas at 340 K this number is 40 (Table 4). In the limit of infinite sampling the simulation at 298 K is expected to show a larger population of the 3_{14}-helix than the simulation at 340 K.

Discussion

A β-peptide with charged side chains such as those of lysine, ornithine or glutamic acid constitutes a more complex folding problem than a β-peptide with only aliphatic substituents. While in the latter case only backbone hydrogen-bond donors and acceptors are present, in a peptide with charged (or polar) side chains, as has been investigated here, the side chains, too, can act as hydrogen-bond donors (lysine and ornithine) or acceptors (glutamic acid). Consequently, the side chain donors or acceptors compete with the backbone hydrogen-bond donor and acceptor atoms, as was observed for peptide **B1** bearing two lysine side chains. Furthermore charged side chains also show salt-bridge interactions among themselves, as well as with the backbone, in particular with the termini. These interactions, side chain-backbone hydro-

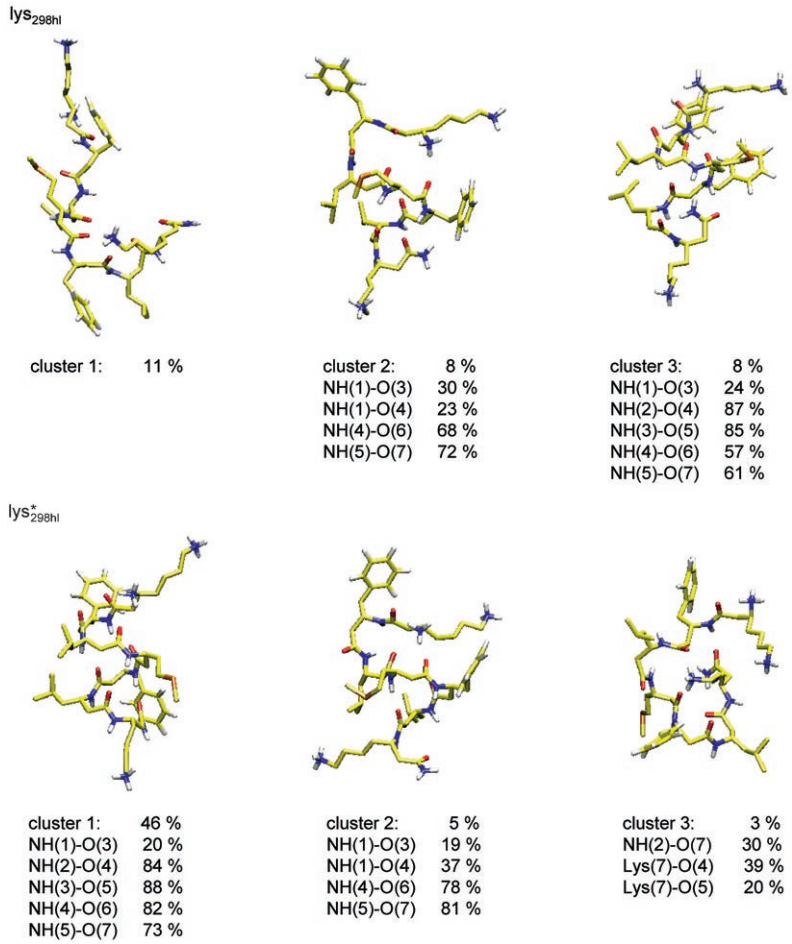

Figure 7. Three most populated conformers (central structures of the three most populated clusters using a backbone (residues 2–6) atom-positional rmsd similarity criterion of 0.1 nm) of peptide **B1** observed in the simulations lys_{298hl} and lys^{*}_{298hl}, where the initial conformation was a canonical 3_{14}-helix, are shown (C = yellow, H = white, N = blue, O = red, S = orange). For each conformer, its corresponding population and the occurrence of the most dominating hydrogen.

gen bonding and salt bridges, can lead to rather stable folding intermediates, which on average results in longer folding times to the "native" conformation than for β-peptides with exclusively aliphatic side chains (Table 4). In the case of peptide **A** in methanol a partly folded 3_{14}-helical conformation is stabilized by a salt-bridge interaction between the ornithine side chain of residue 5 and the C-terminus. In the simulations of peptide **B1** the NH_3^+ group of the lysine at position 7 forms hydrogen bonds or interacts in a salt-bridge-like manner with the carbonyl oxygens of residues 4 and 5 competing with the backbone–backbone hydrogen bonds NH(2)···O(4) and NH(3)···O(5) crucial for the formation of a complete 3_{14}-helix. Similarly, glutamic acid side chains in peptide **C** form hydrogen bonds to the NH groups of the backbone, which might contribute to the observed slowdown of the folding process to the 3_{14}-helix. Once the 3_{14}-helix is formed, its lifetime is, on average, longer than observed for β-peptides with only aliphatic side chains (Tables 4 and 1 in reference [42]). However, this does not apply to most simulations performed for peptide **B1**, where the 3_{14}-helix appears to be rather unstable, probably due to the repulsion between the positively charged lysine side chains in the absence of counterions (see below for a discussion of the effect of counterions). In the case of peptide **A**, the 3_{14}-helix is stabilized by salt-bridge interactions between the ornithine and glutamic-acid side chains at a $i,i\pm3$ position in analogy to salt-bridge interactions in α-helices of α-peptides.[13–16]

Side chain–backbone and side chain–side chain hydrogen bonds are also observed in α-peptides and proteins and have been analyzed in databases of well refined crystallographic protein structures.[64–66] Bordo and Argos[66] report that more than 95% of the observed intra-helix side chain–backbone hydrogen bonds show backward interactions, that is, hydrogen bonds between the side chain at position i and the carbonyl oxygen at position $i-4$ or $i-5$, and are localized mostly at the C-termini of the helices. A similar behavior of the lysine side chains at the C-terminus of β-peptide **B1** is observed in our simulations. Negatively charged residues at or close to the N-terminus ("N-cap") allowing for a favorable interaction with the macrodipole of the α-helix[67–71] also participate in hydrogen bonding with backbone groups.[19,20,72] These side chain–backbone interactions in α-peptides or proteins stabilize the native fold, in this case the α-helical conformation, but possibly also intermediate structures during the folding process. The effect of these side chain–backbone interactions is expected to be more pronounced in methanol than in aqueous solution, since water is a much stronger competitor for hydrogen bonding than methanol, and, thus polar side chains are better solvated in water. Consequently, in the case of β-peptide **A** in water the average folding time to the 3_{14}-helix and its average lifetime are shorter than in methanol (Table 4). Furthermore, the side chain-backbone interactions observed in methanol might be overestimated compared to the real situation, as the simple rigid, non-polarizable methanol model used in the simulation underestimates the dielectric permittivity by roughly 40–50% as do all the available non-polarizable methanol models due to the neglect of the electronic polarizability,[61,73] while the water model used

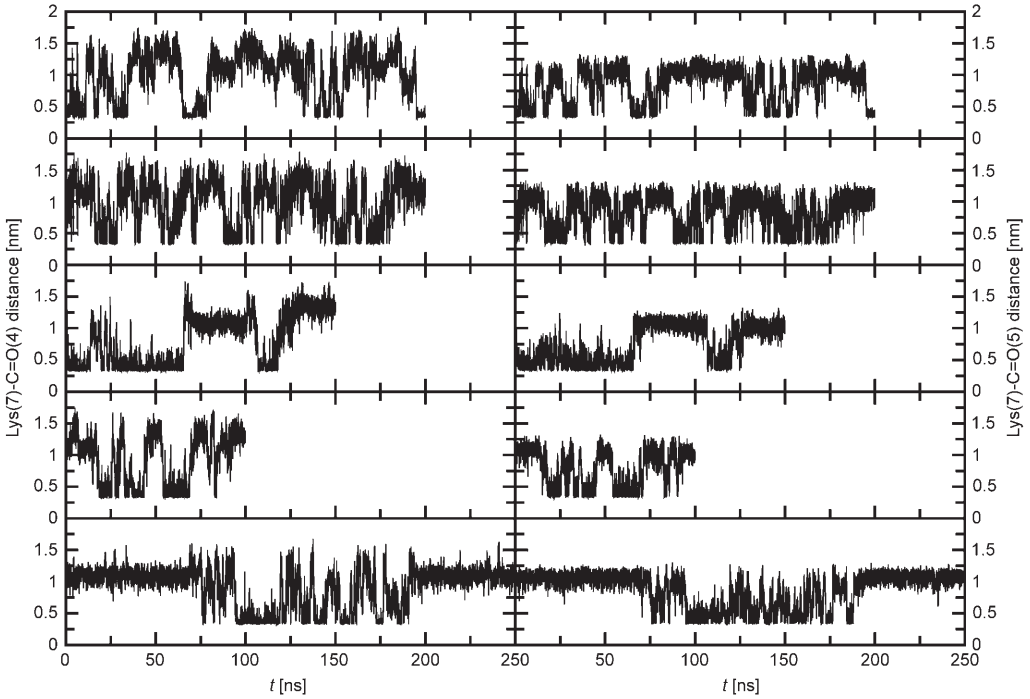

Figure 8. Side chain–backbone interactions between the -NH_3^+ group of the β-lysine residue 7 and the carbonyl groups of residues 4 (left panels) and 5 (right panels) in peptide **B1**. The distances between the centers of geometry of the corresponding GROMOS charge groups are displayed from top to bottom for the simulations lys_{298ext}, lys_{340ext}, lys^*_{298ext}, lys_{298hl}, and lys^*_{298hl} peptide **B1**.

underestimates the dielectric permittivity by only 5%. The poor ability of the solvent methanol to solubilize charged side chains well enough might have an effect on the instability of the 3_{14}-helix observed in most of the simulations of peptide **B1**, as the strong electrostatic interaction between the lysine side chains might disrupt the helical conformation. Yet, this destabilizing effect is not observed when the β-homolysine residues are exchanged for β-homoglutamic acid residues. The most dominant conformer of peptide **C** corresponds to the 3_{14}-helix (Table 4 and Figures 9 and 10) with an average lifetime between 4 and 7 ns, irrespective of the presence of neutralizing counterions.

Intuitively, the destabilizing effect of charged side chains as observed for peptide **B1** is expected to be reduced by the addition of counterions, as was done in simulations lys^*_{298ext}, lys^*_{298hl} and glu^*_{298ext}. While in simulation lys^*_{298hl} starting from the 3_{14}-helical conformation this is clearly the case (compare Figure 5d and e), no significant change in stability of the 3_{14}-helix for peptides **B1** and **C** can be observed in the simulation starting from an extended conformation (Figure 5a and c; Figure 9). As the ions diffuse during the simulation, they are not necessarily always in proximity of the lysine side chains as an analysis of the ion-peptide contacts shows (see Supporting Information for details). Once they move out of the cutoff radius centered around the NH_3^+ group of the lysine side chains, the ions and the NH_3^+ groups do not "see" each other and the ion has no direct effect on the stabilization of the peptide conformation anymore. However, there seems to be no clear correlation between the ion–peptide distances and the stability of the 3_{14}-helical conformation. Clearly, the effect of counterions on the stability or, rather, the conformational distribution of peptides and proteins in simulation is difficult to rationalize from the simulations presented here. It deserves more systematic investigation, for example, as in the studies undertaken by Ibragimova and Wade[74] and Drabik et al.[75]

The fact that charged side chains slow down the kinetics of peptide folding, that is, lengthen the average folding time, has consequences for computational folding studies at the atomistic level. The slower kinetics implies that at a given temperature and within a given simulation time less folding–unfolding events are sampled which implies a slower establishment of conformational equilibrium than in the case of a peptide with exclusively aliphatic residues. Despite their relatively long simulation times, the simulations presented here show a variable degree of convergence.

Peptide **B1** and analogues **C** and **D** adopt right-handed 2.5_{12}-helical conformations in the simulations. However, the populations of the 2.5_{12}-helix are very low and its average lifetime is short, which implies that no detailed conclusions can be drawn about its folding behavior. From the simulations presented here, the 2.5_{12}-helix appears to be certainly less stable than the 3_{14}-helical conformation. Experimentally, the occurrence of 2.5_{12}-helices has only been observed with β-peptides containing mainly *trans*-2-aminocyclopentanecarboxylic acid (*trans*-ACPC) residues.[76,77] Cyclopentane β-amino acid derivatives show a rather high rotational flexibility around the C_β–C_α bond within the conformationally allowed region between minimally 85 and maximally 145° ("pseudorotation" of cyclopentane rings).[91] However, they

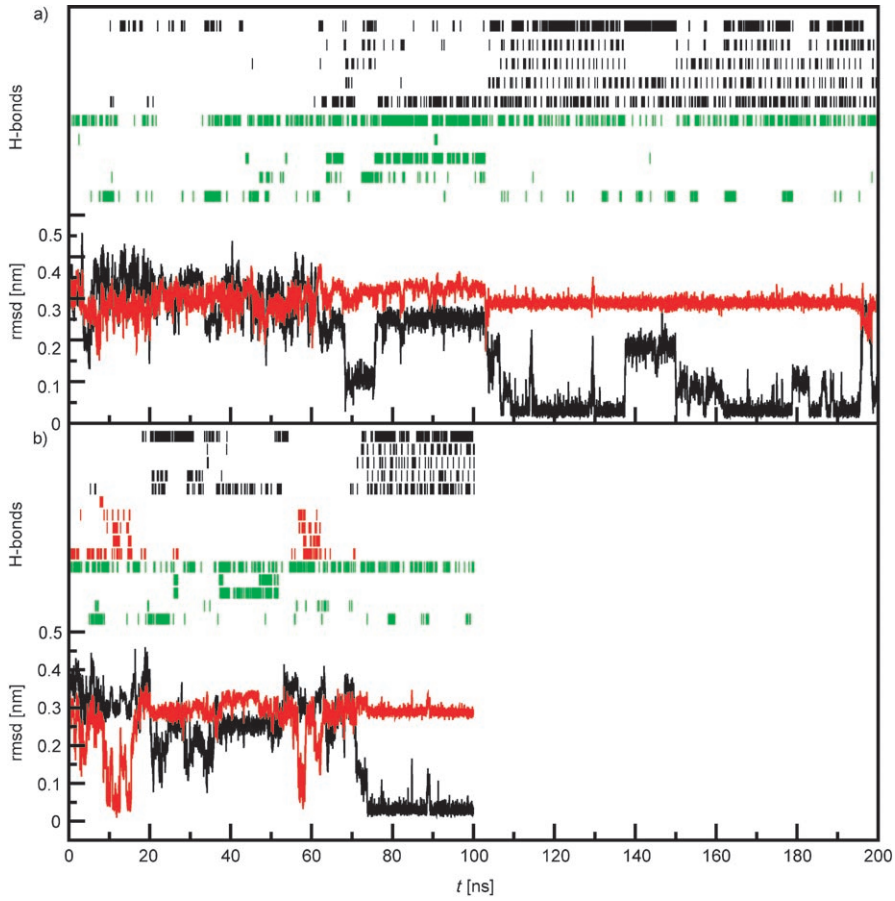

Figure 9. Backbone atom-positional rmsd with respect to a 3_{14}-helical conformation (black) and a 2.5_{12}-helix (red), the two main helical conformations observed in the simulations a) glu_{298ext} and b) glu^{*}_{298ext} of peptide **C**, along with the evolution of the most populated backbone–backbone and side chain–backbone hydrogen bonds. Black: NH(*i*)–O(*i*+2) hydrogen bonds characteristic of 3_{14}-helices. Red: NH(*i*)–O(*i*−3) hydrogen bonds characteristic of 2.5_{12}-helices; Green: Side chain-backbone hydrogen bonds between the glutamic acid side chains and the NH groups, displayed from top to bottom: NH(1)–Glu(1), NH(2)–Glu(7), NH(3)–Glu(7), NH(4)–Glu(7), NH(7)–Glu(7). For more information see captions of Figure 5 and Table 2.

can never adopt the two extreme values of 60° ((+)-synclinal, (+)-sc) and 180° (antiperiplanar, ap) as in open-chain or cyclohexane derivatives (Figure 13). Thus, β-peptides built from *trans*-ACPC residues cannot adopt a 3_{14}-helix or a 12/10-helix ((+)-sc), where the dihedral angle -NH-C_β-C_α-CO- is about 60°. In 2.5_{12}-helices the values for this dihedral angle are larger than 60° and can vary between 87 and 155° as in the crystal structure of a β-octapeptide consisting of *trans*-2-aminocyclopentanecarboxylic acid residues (*trans*-ACPC)[76,77] or between 70 and 135° as in the 2.5_{12}-helical structures observed in our simulations (see Figure 13). In contrast to the cyclopentane derivatives the rotational barrier between the synclinal and antiperiplanar conformations in open-chain and cyclohexane β-amino acid moieties is much higher. The NH-C-C-CO dihedral angle in the simulation of 3_{14}-helices is close to +60°.[54] Ab initio calculations in vacuo of β-peptide models suggest that a right-handed 2.5_{12}-helix of β-peptides, built of *(S)*-β-amino acids is equally favorable as a left-handed 3_{14}-helix.[78,79] While the 3_{14}-helix is thought to be most favored in terms of torsional interactions, the 2.5_{12}-helix is suggested to benefit most from inter-residue electrostatic interactions.[79] According to a recent MD simulation study of a hydroxylated peptide, the 2.5_{12}-helix is the most stable conformer.[80]

Conclusion

The conformational and dynamic behavior of the four different β-peptides **A**–**D** in methanol and water (Figure 1) has been analyzed by molecular dynamics simulation in order to study the influence of charged side chains on the folding–unfolding equilibrium. All four peptides are expected to adopt a left-handed 3_{14}-helical conformation in solution. According to our simulations, the presence of charged side chains leads to relatively stable intermediate conformations in methanol, due to side chain–backbone interactions such as hydrogen bonds or salt bridges, which are competing with the backbone–backbone hydrogen bonds. Similar interactions are observed experimentally in α-peptides and proteins, where they stabilize the N- and C-caps of α-helices. Consequently, the presence of charged side chains in β-pep-

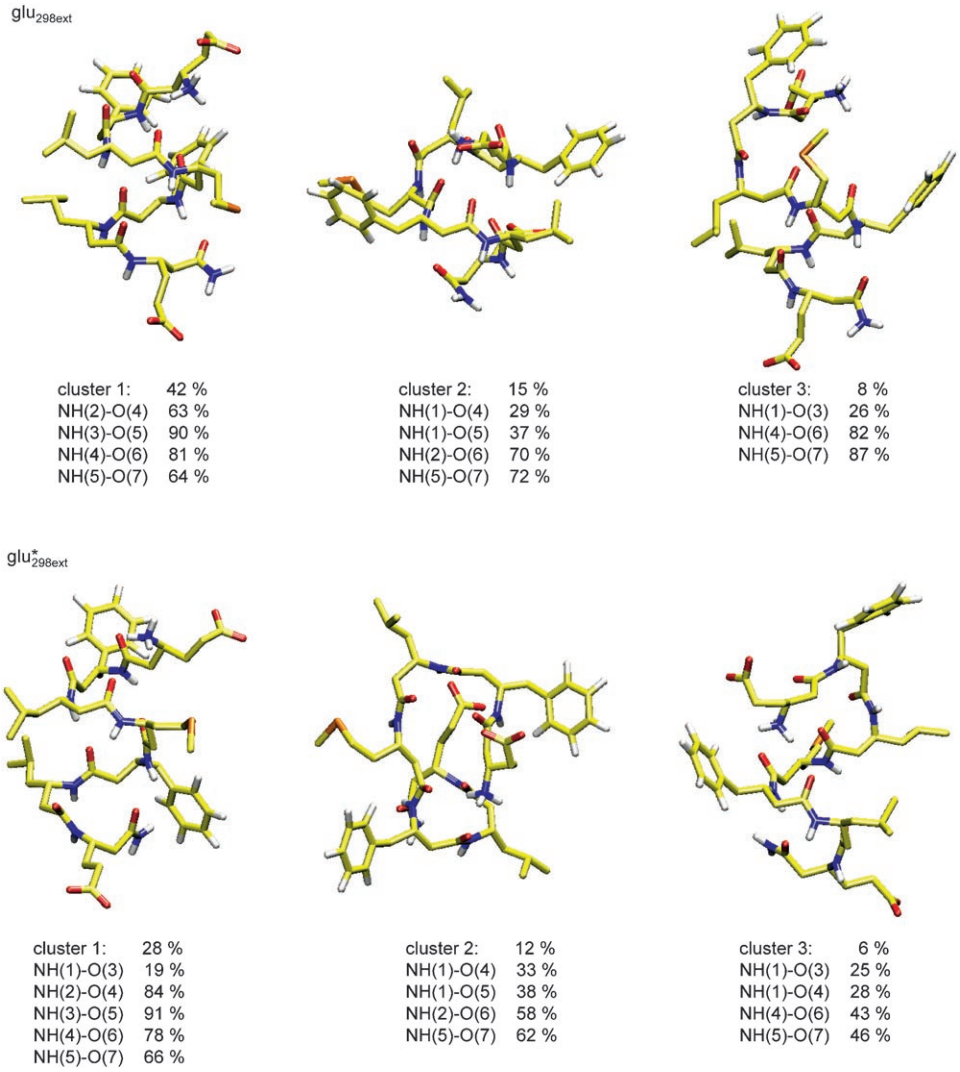

Figure 10. Three most populated conformers (central structures of the three most populated clusters using a backbone (residues 2–6) atom-positional rmsd similarity criterion of 0.1 nm) of peptide **C** observed in the simulations in methanol at 298 K without (glu_{298ext}) and with neutralizing counterions (glu^{*}_{298ext}) (C = yellow, H = white, N = blue, O = red). For each conformer, the corresponding population and the occurrence of the most dominating hydrogen bonds are indicated. For nomenclature see caption of Table 2.

tides significantly slows down the folding process and, within a given sampling time, fewer folding events can be observed compared to the folding of a β-peptide carrying aliphatic side chains only. Therefore, longer sampling times are required for convergence and to investigate reversible peptide folding. This decelerating effect on the folding behavior is found to be more pronounced in methanol than in water, and in the presence of lysine side chains, where the entropic loss of the side chains upon folding might have an influence.[25,81] Salt bridges between side chains (peptide **A**) are observed to stabilize the "native" fold, but do not appear to be a major driving force for folding, that is, also in that case relatively long average folding times are observed in methanol.

Furthermore, we note that β-peptides bearing only (*S*)-substituents on the β-carbon preferentially adopt a left-handed 3_{14}-helix in solution, which is in line with many experimental studies.[39,52,62,63] The occasionally observed right-handed 2.5_{12}-helical conformations in the simulations appear to be rather unstable. The experimental data for peptide **A** were largely reproduced in the simulations, although lack of convergence of the folding–unfolding equilibrium in methanol causes NOE distance-bound violations of 14 out of 29 NOE distances up to 0.29 nm. In water only 5 out of 21 NOE distances are violated with a largest value of 0.17 nm. The $^{3}J(NH,C_{\beta}H)$ coupling constants are well reproduced in the simulations. For peptide **B2** (carboxylated C-terminus) it is not possible to determine a predominant solution structure from the available NMR data. Nevertheless, we note that the simulation of peptide **B1** (with C-terminal amide group) with the largest population of the 3_{14}-helix fulfils the experimentally inferred NOE upper bound distances and

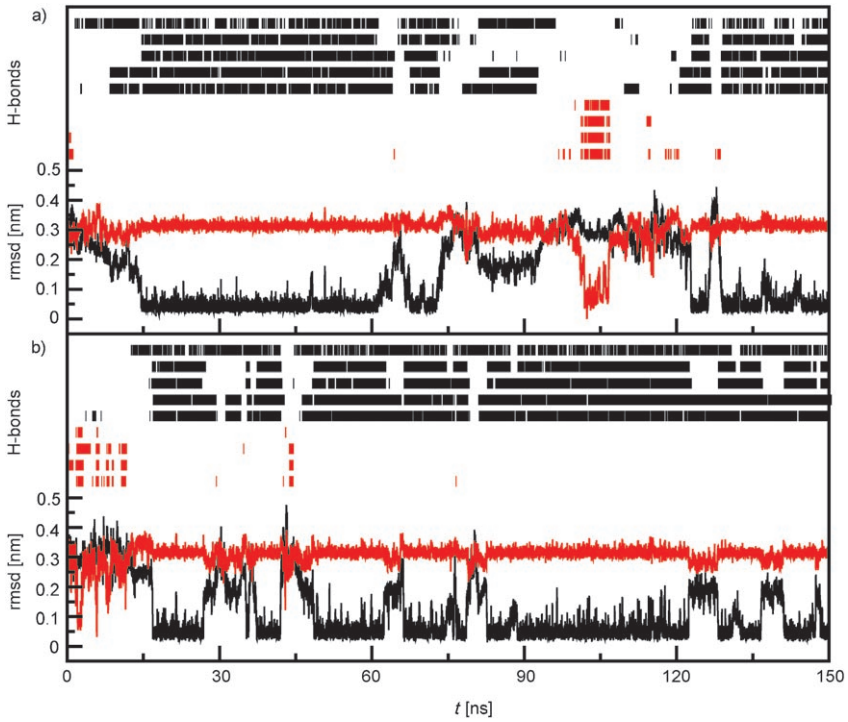

Figure 11. Backbone atom-positional rmsd with respect to a 3_{14}-helical conformation (black) and a 2.5_{12}-helix (red), the two main helical conformations observed in the simulations a) val_{298ext} and b) val_{340ext} of peptide **D**, along with the evolution of the most populated backbone-backbone hydrogen bonds. Black: NH(*i*)–O(*i*+2) hydrogen bonds characteristic of 3_{14}-helices; Red: NH(*i*)–O(*i*–3) hydrogen bonds characteristic of 2.5_{12}-helices. For more information see caption of Figure 5 and Table 2.

the experimental ^3J coupling constants better than the four simulations with a significantly lower population of the 3_{14}-helix.

Methods

Computational methods

Molecular model: The β-peptides were modeled using the GROMOS96 biomolecular force field, parameter set 45A3.[56,58] Aliphatic CH_n groups were treated as united atoms, both in the peptides and the solvent. The protonation states of the acidic and basic groups were inferred from the procedures of the synthesis and purification of the peptides: The N-termini and the β-ornithine and β-lysine side chains were protonated, whereas the C-terminus of peptide **A** and the β-glutamate side chains were deprotonated. Methanol and water were modeled as rigid three-point models using the SPC/L water model[82] and the standard GROMOS96 methanol model,[56] respectively.

Simulation setup: All MD simulations presented here were carried out using the GROMOS96 program.[56,57] They are summarized in Table 1. For the simulations starting from a fully extended peptide conformation (simulations orn–glu_{MeOH}, orn–glu_{H_2O}, lys_{298ext}, lys_{340ext}, lys^*_{298ext}, glu_{298ext}, glu^*_{298ext}, val_{298ext} and val_{340ext}) all backbone dihedral angles were set to 180° and the side chain dihedral angles were randomly taken from the possible rotamers. The peptide was then solvated in a truncated-octahedron-shaped box. The size of the box was chosen such that the initial minimum distance between peptide atoms and the square walls of the truncated octahedron was 1.4 nm. In the case where the starting structure was a 3_{14}-helix (simulations lys_{298hl} and lys^*_{298hl}) the peptide was put in a rectangular box assuring a minimum distance of 1.5 nm to the walls. Periodic boundary conditions were applied. To obtain the systems lys^*_{298ext} and lys^*_{298hl}, three methanol molecules experiencing the largest positive Coulomb potential were replaced by three chlorine ions to neutralize the system. Similarily, two sodium ions and one chlorine ion were replacing three methanol molecules to obtain the system glu^*_{298ext}.

After relaxation of the systems using steepest descent energy minimization, the MD simulations were started by taking the initial velocities from Maxwellian distributions at 298 or 340 K for the systems where the peptides are fully extended and at 50 K for the systems starting from a left-handed 3_{14}-helical conformation. Solvent and solute were independently coupled to a temperature bath with a relaxation time of 0.1 ps.[83] The pressure was calculated with a molecular virial and held constant by weak coupling to a pressure bath with a relaxation time of 0.5 ps and using an isothermal compressibility of 4.575×10^{-4} $(kJ\,mol^{-1}\,nm^{-3})^{-1}$ and 7.768×10^{-4} $(kJ\,mol^{-1}\,nm^{-3})^{-1}$ for the simulations in methanol and water, respectively. Bond lengths were constrained using the SHAKE algorithm[84] with a geometric tolerance of 10^{-4}. The equations of motion were integrated using the leap-frog algorithm and a time step of 2 fs. The interaction between atoms in so-called charge groups[56] was calculated according to a spherical triple-range cutoff scheme: Short-range van der Waals and electrostatic interactions were evaluated at every time step by using a charge-group pair list that was generated with a short-range cutoff radius of 0.8 nm between the centers of geometry of the peptide charge groups and the oxygen atoms of the methanol or water solvent molecules. Longer-range van der Waals and electrostatic interactions, between pairs at a distance longer than 0.8 nm and shorter than a long-range cutoff of 1.4 nm, were evaluated every fifth time step, at which point the pair list was also updated, and were kept unchanged between these updates. To approximate the electrostatic interactions beyond the long-range cutoff, a Poisson–Boltzmann reaction field force was used. The value for the dielectric permittivity of the continuum outside the long-range cutoff was set to 17.7 and 73.5, corresponding to the values for the dielectric permittivity of the methanol model[61] and water

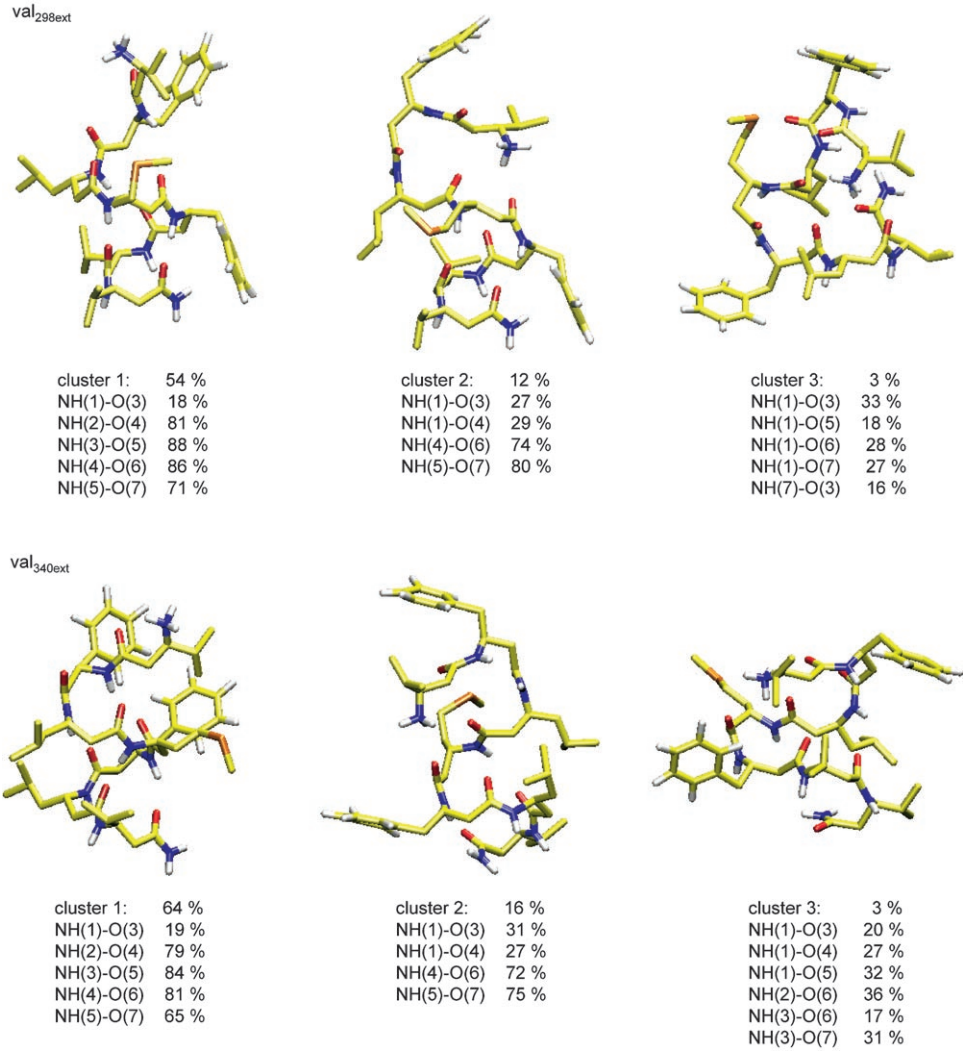

Figure 12. Three most populated conformers (central structures of the three most populated clusters using a backbone (residues 2–6) atom-positional rmsd similarity criterion of 0.1 nm) of peptide **D** observed in the simulations in methanol at 298 K (val_{298ext}) and 340 K (val_{340ext}) (C = yellow, H = white, N = blue, O = red). For each conformer, the corresponding population and the occurrence of the most dominating hydrogen bonds are indicated. For nomenclature see caption of Table 2.

model[82] employed, respectively. In the simulations starting from a 3_{14}-helical conformation (simulations lys_{298hl} and lys^{*}_{298hl}) the positions of the atoms of the peptides were initially restrained using a harmonic restraining force with a force constant of 10^4 kJ mol^{-1} nm^{-2} during the first 50 ps of simulation. During that period of time the temperature was stepwise increased to 298 K and the restraining force gradually decreased. The simulations were equilibrated for 1 ns and the following 50 to 250 ns were used for analysis saving configurations every 0.5 ps.

Analysis: Least-squares translational and rotational fitting of atomic coordinates for the calculation of the root-mean-square-differences (rmsd) was based on the backbone atoms (N, C_β, C_α, C) of residues 2 to 6. A conformational clustering analysis was performed as described by Daura et al.[85] on a set of 10^4 peptide structures taken at 0.01 ns intervals from the simulation. The backbone atom-positional rmsd was used as similarity criterion. A maximum cluster radius of 0.1 nm was chosen.[40,85] Hydrogen bonds were calculated using a geometric criterion. A hydrogen bond is defined by a minimum donor-hydrogen-acceptor angle of 135° and a maximum hydrogen-acceptor distance of 0.25 nm. Salt bridges were determined using a distance criterion. Two (GROMOS) charge groups[56] are considered to form a salt bridge, if their centers of geometry are not more than 0.5 nm apart.

Interproton distances derived from the NOE intensities at 298 K were compared to the corresponding average effective interproton distances in the simulations calculated using $\langle r^{-6}\rangle^{-1/6}$ averaging of the instantaneous interproton distances r. The experimental NOE intensities have been classified in three r_{exptl} distance categories: strong (s) with $r_{exptl} \leq 0.3$ nm, medium (m) with $r_{exptl} \leq 0.35$ nm, and weak (w) with $r_{exptl} \leq 0.45$ nm. As in the GROMOS96 biomolecular force field the aliphatic hydrogen atoms are treated within a united atom model, the interproton distances involving aliphatic hydrogen atoms were calculated by defining virtual (for CH_1 and prochiral CH_2) and pseudo (for CH_3 and non-stereospecific CH_2) atomic positions at the time of analysis.[56] The pseudo-atom NOE distance bound corrections of reference gromos:96 were used. ^3J coupling constants were calculated from the simulation using the Karplus relation:[59]

$$^3J(\mathrm{H,H}) = a\cos^2\theta + b\cos\theta + c \quad (1)$$

where a, b and c were chosen equal to 6.4, −1.4, and 1.9 Hz, respectively,

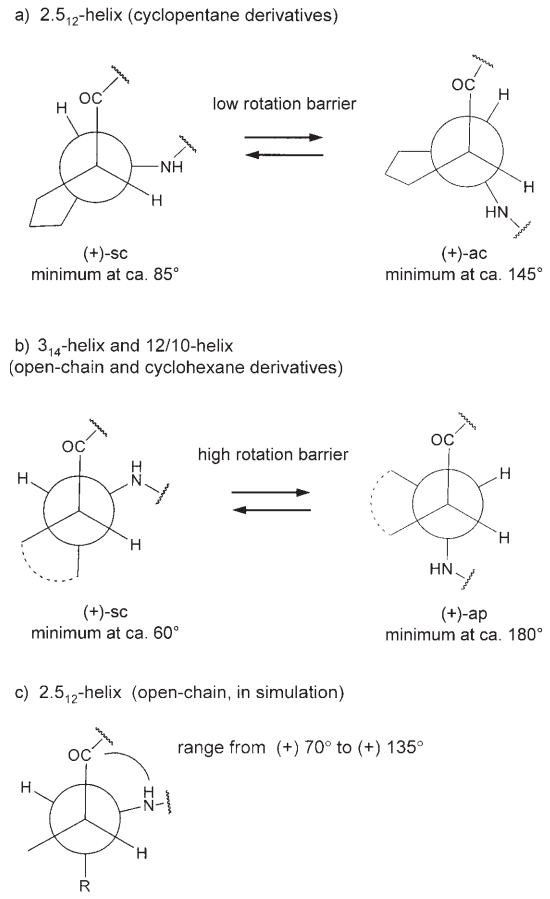

Figure 13. Comparison of the backbone dihedral-angle conformation of a) cyclopentane and open-chain or cyclohexane β-amino acid derivatives (b, c).

for the calculation of ^3J(NH,CH)[86] and equal to 9.5, −1.6, and 1.8 Hz for the calculation of ^3J(CH,CH).[87] In the case of peptide **B1** an alternative set of coefficients for the Karplus relation was used in addition (for reasons of comparison) to calculate the ^3J coupling constants, namely $a=6.7$, $b=-1.3$ and $c=1.5$ Hz for ^3J(NH,CH)[88] and $a=9.6$, $b=-1.0$, and $c=$ 1.2 Hz for ^3J(CH,CH).[89]

For a description of the synthesis, characterization and NMR analysis of peptide **B2**, please see the Supporting Information.

Acknowledgements

Financial support was obtained through the National Center of Competence in Research (NCCR) Structural Biology of the Swiss National Science Foundation, which is gratefully acknowledged. X.D. acknowledges support from the Catalan DURSI, grant 2002PIRA-00007, and the Spanish MCYT/FEDER, grant BIO2003-02848. D.S. thanks the Swiss National Science Foundation (Project No. 2000-058831.99) and Novartis Pharma AG for financial support.

[1] P. C. Lyu, M. I. Liff, L. A. Marky, N. R. Kallenbach, *Science* **1990**, *250*, 669–673.
[2] S. Padmanabhan, S. Marqusee, T. Ridgeway, T. M. Laue, R. L. Baldwin, *Nature* **1990**, *344*, 268–270.
[3] K. T. O'Neil, W. F. DeGrado, *Science* **1990**, *250*, 646–651.
[4] L. Serrano, *Adv. Protein Chem.* **2000**, *53*, 49–85.
[5] B. Rost, *J. Struct. Biol.* **2001**, *134*, 204–218.
[6] A. J. Doig, *Biophys. Chem.* **2002**, *101*, 281–293.
[7] A. Kidera, Y. Konishi, M. Oka, T. Ooi, H. A. Scheraga, *J. Protein Chem.* **1985**, *4*, 23–55.
[8] K. A. Dill, *Biochemistry* **1990**, *29*, 7133–7155.
[9] S. Padmanabhan, R. L. Baldwin, *J. Mol. Biol.* **1991**, *219*, 135–137.
[10] M. Blaber, X. Zhang, B. W. Matthews, *Science* **1993**, *260*, 1637–1640.
[11] S. Padmanabhan, R. L. Baldwin, *Protein Sci.* **1994**, *3*, 1992–1997.
[12] K. A. Dill, K. M. Fiebig, H. S. Chan, *Proc. Natl. Acad. Sci. USA* **1993**, *90*, 1942–1946.
[13] S. Marquese, R. L. Baldwin, *Proc. Natl. Acad. Sci. USA* **1987**, *84*, 8898–8902.
[14] G. Merutka, E. Stellwagen, *Biochemistry* **1991**, *30*, 1591–1594.
[15] G. Merutka, W. Shalongo, E. Stellwagen, *Biochemistry* **1991**, *30*, 4245–4248.
[16] B. M. P. Huyghues-Despointes, J. M. Scholtz, R. L. Baldwin, *Protein Sci.* **1993**, *2*, 80–85.
[17] B. M. P. Huyghues-Despointes, T. M. Klingler, R. L. Baldwin, *Biochemistry* **1995**, *34*, 13267–13271.
[18] B. J. Stapley, A. J. Doig, *J. Mol. Biol.* **1997**, *272*, 465–473.
[19] J. S. Richardson, D. C. Richardson, *Science* **1988**, *240*, 1648–1652.
[20] L. Serrano, A. E. Fersht, *Nature* **1989**, *342*, 296–299.
[21] B. J. Stapley, A. J. Doig, *J. Mol. Biol.* **1997**, *272*, 456–464.
[22] T. P. Creamer, G. D. Rose, *Proc. Natl. Acad. Sci. USA* **1992**, *89*, 5937–5941.
[23] T. P. Creamer, G. D. Rose, *Proteins Struct. Funct. Genet.* **1994**, *19*, 85–97.
[24] T. P. Creamer, G. D. Rose, *Protein Sci.* **1995**, *4*, 1305–1314.
[25] T. P. Creamer, *Proteins Struct. Funct. Genet.* **2000**, *40*, 443–450.
[26] L. Piela, G. Nemethy, H. A. Scheraga, *Biopolymers* **1987**, *26*, 1273–1286.
[27] R. H. Yun, J. Hermans, *Protein Eng.* **1991**, *4*, 761–766.
[28] R. H. Yun, A. Anderson, J. Hermans, *Proteins Struct. Funct. Genet.* **1991**, *10*, 219–228.
[29] J. Hermans, A. G. Anderson, R. H. Yun, *Biochemistry* **1992**, *31*, 5646–5653.
[30] Y. Bai, S. W. Englander, *Proteins Struct. Funct. Genet.* **1994**, *18*, 262–266.
[31] F. Avbelj, J. Moult, *Biochemistry* **1995**, *34*, 755–764.
[32] F. Avbelj, L. Fele, *J. Mol. Biol.* **1998**, *279*, 665–684.
[33] F. Avbelj, *J. Mol. Biol.* **2000**, *300*, 1335–1359.
[34] L. Baltzer, H. Nillson, J. Nillson, *Chem. Rev.* **2001**, *101*, 3153–3163.
[35] T. M. Penning, *Chem. Rev.* **2001**, *101*, 3027–3046.
[36] J. Venkatraman, S. C. Shankaramma, P. Balaram, *Chem. Rev.* **2001**, *101*, 3131–3152.
[37] D. J. Hill, M. J. Mio, R. B. Prince, T. S. Hughes, J. S. Moore, *Chem. Rev.* **2001**, *101*, 3893–4011.
[38] R. P. Cheng, S. H. Gellman, W. F. DeGrado, *Chem. Rev.* **2001**, *101*, 3219–3232.
[39] D. Seebach, J. L. Matthews, *Chem. Commun.* **1997**, *79*, 2015–2022.
[40] X. Daura, B. Jaun, D. Seebach, W. F. van Gunsteren, A. E. Mark, *J. Mol. Biol.* **1998**, *280*, 925–932.
[41] W. F. van Gunsteren, R. Bürgi, C. Peter, X. Daura, *Angew. Chem.* **2001**, *113*, 363–367; *Angew. Chem. Int. Ed.* **2001**, *40*, 351–355.
[42] X. Daura, A. Glättli, P. Gee, C. Peter, W. F. van Gunsteren, *Adv. Protein Chem.* **2002**, *62*, 341–360.
[43] D. Seebach, M. Overhand, F. N. M. Kühnle, B. Martinoni, L. Oberer, U. Hommel, H. Widmer, *Helv. Chim. Acta* **1996**, *79*, 913–941.
[44] D. Seebach, P. E. Ciceri, M. Overhand, B. Jaun, D. Rigo, L. Oberer, U. Hommel, H. Widmer, *Helv. Chim. Acta* **1996**, *79*, 2043–2066.
[45] X. Daura, W. F. van Gunsteren, D. Rigo, B. Jaun, D. Seebach, *Chem. Eur. J.* **1997**, *3*, 1410–1417.
[46] D. Seebach, S. Abele, K. Gademann, G. Guichard, T. Hintermann, B. Jaun, J. L. Matthews, J. V. Schreiber, L. Oberer, U. Hommel, H. Widmer, *Helv. Chim. Acta* **1998**, *81*, 932–982.

[47] X. Daura, K. Gademann, B. Jaun, D. Seebach, W. F. van Gunsteren, A. E. Mark, *Angew. Chem.* **1999**, *111*, 249–253; *Angew. Chem. Int. Ed.* **1999**, *38*, 236–240.
[48] D. Seebach, S. Abele, K. Gademann, B. Jaun, *Angew. Chem.* **1999**, *111*, 1700–1703; *Angew. Chem. Int. Ed.* **1999**, *38*, 1595–1597.
[49] X. Daura, K. Gademann, H. Schäfer, B. Jaun, D. Seebach, W. F. van Gunsteren, *J. Am. Chem. Soc.* **2001**, *123*, 2393–2404.
[50] J. L. Matthews, K. Gademann, B. Jaun, D. Seebach, *J. Chem. Soc. Perkin Trans. 1* **1998**, 3331–3340.
[51] Y. Hamuro, J. P. Schneider, W. F. DeGrado, *J. Am. Chem. Soc.* **1999**, *121*, 12200–12201.
[52] P. I. Arvidsson, M. Rueping, D. Seebach, *Chem. Commun.* **2001**, *7*, 649–650.
[53] T. L. Raguse, J. R. Lai, S. H. Gellman, *Helv. Chim. Acta* **2002**, *85*, 4154–4164.
[54] A. Glättli, D. Seebach, W. F. van Gunsteren, *Helv. Chim. Acta* **2004**, *87*, 2487–2506.
[55] D. Seebach, J. V. Schreiber, S. Abele, X. Daura, W. F. van Gunsteren, *Helv. Chim. Acta* **2000**, *83*, 34–56.
[56] W. F. van Gunsteren, S. R. Billeter, A. A. Eising, P. H. Hünenberger, P. Krüger, A. E. Mark, W. R. P. Scott, I. G. Tironi, *Biomolecular Simulation: The GROMOS96 Manual and User Guide*, vdf Hochschulverlag, ETH Zürich, Switzerland, **1996**.
[57] W. R. P. Scott, P. H. Hünenberger, I. G. Tironi, A. E. Mark, S. R. Billeter, J. Fennen, A. E. Torda, T. Huber, P. Krüger, W. F. van Gunsteren, *J. Phys. Chem.* **1999**, *103*, 3596–3607.
[58] L. D. Schuler, X. Daura, W. F. van Gunsteren, *J. Comput. Chem.* **2001**, *22*, 1205–1218.
[59] M. Karplus, *J. Chem. Phys.* **1959**, *30*, 11–15.
[60] K. Wüthrich, *NMR of Protein and Nucleic Acids*, Wiley-VCH, New York, USA, **1986**.
[61] R. Walser, A. E. Mark, W. F. van Gunsteren, M. Lauterbach, G. Wipff, *J. Chem. Phys.* **2000**, *112*, 10450–10459.
[62] W. F. DeGrado, J. P. Schneider, Y. Hamuro, *J. Pept. Res.* **1999**, *54*, 206–217.
[63] K. Gademann, T. Hintermann, J. V. Schreiber, *Curr. Med. Chem.* **1999**, *6*, 905–925.
[64] N. E. Baker, R. E. Hubbard, *Prog. Biophys. Mol. Biol.* **1984**, *44*, 97–179.
[65] D. F. Stickle, L. G. Presta, K. A. Dill, G. D. Rose, *J. Mol. Biol.* **1992**, *226*, 1143–1159.
[66] D. Bordo, P. Argos, *J. Mol. Biol.* **1994**, *243*, 504–519.
[67] A. Wada, *Adv. Biophys.* **1976**, *9*, 1–63.
[68] W. G. J. Hol, P. T. van Duijnen, H. J. C. Berendsen, *Nature* **1978**, *273*, 443–446.
[69] J. Warwicker, H. C. Watson, *J. Mol. Biol.* **1982**, *157*, 671–679.
[70] W. G. J. Hol, L. M. Halie, *Nature* **1981**, *294*, 532–536.
[71] W. G. J. Hol, *Prog. Biophys. Mol. Biol.* **1985**, *45*, 149–195.
[72] E. T. Harper, G. D. Rose, *Biochemistry* **1993**, *32*, 7605–7609.
[73] H. Yu, W. F. van Gunsteren, unpublished results, **2005**.
[74] G. T. Ibragimova, R. C. Wade, *Biophys. J.* **1998**, *74*, 2906–2911.
[75] P. Drabik, A. Liwo, C. Czaplewski, J. Ciarkowski, *Protein Eng.* **2001**, *2001*, 747–752.
[76] D. H. Appella, L. A. Christianson, D. A. Klein, D. R. Powell, X. Huang, J. J. Brachi Jr., S. H. Gellman, *Nature* **1997**, *387*, 381–384.
[77] D. H. Appella, L. A. Christianson, I. L. Karle, D. R. Powell, S. H. Gellman, *J. Am. Chem. Soc.* **1999**, *121*, 6206–6212.
[78] R. Günther, H.-J. Hofmann, *Helv. Chim. Acta* **2002**, *85*, 2149–2168.
[79] Y.-D. Wu, J.-Q. Lin, Y.-L. Zhao, *Helv. Chim. Acta* **2002**, *85*, 3144–3160.
[80] A. Glättli, W. F. van Gunsteren, *Angew. Chem.* **2004**, *116*, 6472–6476; *Angew. Chem. Int. Ed.* **2004**, *43*, 6312–6316.
[81] A. J. Doig, M. J. E. Sternberg, *Protein Sci.* **1995**, *4*, 2247–2251.
[82] A. Glättli, X. Daura, W. F. van Gunsteren, *J. Chem. Phys.* **2002**, *116*, 9811–9828.
[83] H. J. C. Berendsen, J. P. M. Postma, W. F. van Gunsteren, A. DiNola, J. R. Haak, *J. Chem. Phys.* **1984**, *81*, 3684–3690.
[84] J.-P. Ryckaert, G. Ciccotti, H. J. C. Berendsen, *J. Comput. Phys.* **1977**, *23*, 327–341.
[85] X. Daura, W. F. van Gunsteren, A. E. Mark, *Proteins Struct. Funct. Genet.* **1999**, *34*, 269–280.
[86] A. Pardi, M. Billeter, K. Wüthrich, *J. Mol. Biol.* **1984**, *180*, 741–751.
[87] A. de Marco, M. Llinás, K. Wüthrich, *Biopolymers* **1978**, *17*, 617–636.
[88] S. Ludvigsen, K. V. Andersen, F. M. Poulsen, *J. Mol. Biol.* **1991**, *217*, 731–736.
[89] C. A. G. Haasnoot, F. A. A. M. de Leeuw, C. Altona, *Tetrahedron* **1989**, *36*, 2783–2791.
[90] M. A. Rueping, *Synthesis, Structural and Biological Aspects of Oligo(3-hydroxybutanoates) and of β- and γ-Peptides*, Ph. D. thesis, Diss. ETH No. 14677, ETH Zürich, Switzerland, **2002**.
[91] G. Quinkert, E. Egert, C. Griesinger, *Aspects of Organic Chemistry - Structure*, Verlag Helvetica Chimica Acta, Basel, Switzerland, **1996**.

Received: November 8, 2004
Revised: May 4, 2005
Published online: October 25, 2005

